

# Referee1

Interactive comment on

"Linkage between Dust Cycle and Loess of the Last Glacial Maximum in Europe"

by Erik Jan Schaffernicht et al.

Anonymous Referee #1 Received and published: 23 October 2019

Comments to "Linkage between Dust Cycle and Loess of the Last Glacial Maximum in Europe" by Schaffernicht et al.

Manuscript number: acp-2019-693

R= Referee1

A= Authors' reply

R:

Quantification of the dust cycle for the Last Glacial Maximum (LGM) is crucial to better understand effects of dust on glacial paleoclimate and paleoenvironments. Loess deposits are paleodust archives providing basic information to test dust cycle models such as the one introduced by Schaffernicht et al. This dust cycle simulation is novel in the sense that it follows a weather typing approach (circulation weather type, CWT, classification) providing deeper insight into regional differences of peak glacial atmospheric circulation in Europe and dust emission/deposition in relation to CWT classes. As demonstrated by the authors simulated bulk and dust MAR values are in good agreement with the paleodust record (loess MARs) in central Europe, and this study reveals the significant role of easterly and cyclonic wind regimes in LGM dust emission and dust emission/deposition seasonalities (summer/autumn peak). My limited number of (minor) comments/suggestions can be found below as line-by-line comments. This manuscript is recommended for publication in ACP after minor revisions.

A:

We thank Referee1 very much for the suggestions and comments on our manuscript as they contribute to improving the submitted manuscript. Our point by point answers to Referee1's comments follow.

## Specific comments

R1.1 Lines 41-46: Bulk and dust MARs should clearly be distinguished in this paragraph, and later in the text.

A These terms are consistently used in the complete manuscript:

1) "MAR":

MAR is equivalent to "bulk MAR". It refers only to fieldwork-based reconstructed accumulations rates without any limitation of particle size.

2) "MAR10":

MAR10 refers only to fieldwork-based reconstructed accumulation rates of particles up to 10 micron diameter.

3) "dust deposition rates":

This term refers to only any kind of numerical-model simulated deposition rate without limiting or specifying its particle size range. For example, the particle sizes range in the WRF-Chem-LGM includes particles up to 20 micron.

4a) " $F_{D20}$ ":

It labels the WRF-Chem-LGM simulated deposition rates up to 20 micron particle size.

4b) " $F_{D12}$ ":

It labels the WRF-Chem LGM simulated deposition rates up to 12 micron particle size.

4c) " $F_D$ ":

It refers to  $F_{D20}$  and  $F_{D12}$ .

R1.2 The dust MAR value (100 g/m<sup>2</sup>/yr) in line 43 is slightly misleading, as this is an estimate of MAR of the <10 micron fraction, so cannot be directly compared to bulk MAR (800 g/m<sup>2</sup>/yr), as given in the next sentence.

A Referee1 claims that the 100g/m<sup>2</sup>/yr (i.e. the upper limit of the numerically-simulated deposition rates of the cited studies) is an estimate based only on MAR10 (= "MAR of the < 10 micron fraction").

This is not the case, i.e.: The 100g/m<sup>2</sup>/yr are no estimate of the MAR10.

Reasoning:

Only two of the five references that we cite to prove our statement are based on simulating particles < 10micron. In one of the remaining three references, for example, the particle size is limited by 1000micron.

In summary, the 100 g/m<sup>2</sup>/yr bases on at least five published simulation results, all of which differ from one another in their particle size ranges. This upper deposition rate limit (= 100 g/m<sup>2</sup>/yr) can thus not be related to a common particle size range. At least two studies explicitly use a particle size range that exceeds 10 microns.

Thus, our statement that the numerical simulations published up to now significantly underestimate the field research-based reconstructed accumulation rates for the LGM, remains valid.

R1.3 Lines 150-151: Significant loess accumulations are found along the west bank of the Danube river in Hungary, Croatia and Serbia, providing further observational evidence for easterly paleowinds.

A Referee1's statement is very much appreciated. If Referee1 provides us with a full reference to a peer-reviewed article confirming this, we will be happy to include this loess-related statement in the manuscript.

R1.4 Figure 4:

a) Position of the scale is inappropriate as it covers circles representing MAR magnitudes.

A The position of colour bar was intentionally set like this to provide more space for the important content, i.e. the panels showing the maps. This design was chosen because the order of magnitude of the MARs are represented solely by the diameter of their circles. It is therefore sufficient to display only two thirds of a full circle line to uniquely define and recognize its diameter.

However, if Referee1 (after reading this reasoning) continues to insist that all circles are shown completely above the colour bar (which means that the main content of the figure is reduced), we will comply to his/her request.

R1.5 b) Also, I suggest adding an x-x plot directly showing a model/paleodata comparison of dust MAR values.

A Such an x-x plot (R1.5-Fig. 1) showing the WRF-Chem-LGM-based dust deposition rates compared to the MARs can be found below.

The x-x plot shows that the WRF-Chem-LGM based dust deposition rates are in good agreement with the fieldwork-based reconstructed MARs. Ultimately, it must be taken into account that the reconstructed MARs for certain areas show great local variability, the cause of which is probably due to conditions that can still not be completely resolved in the applied WRF-Chem-LGM grid. It is therefore possible that some small-scale features cannot be reproduced in the grid resolution of this study. In addition, the small-scale land surface conditions in Europe during the LGM are so far not sufficiently known nor researched.

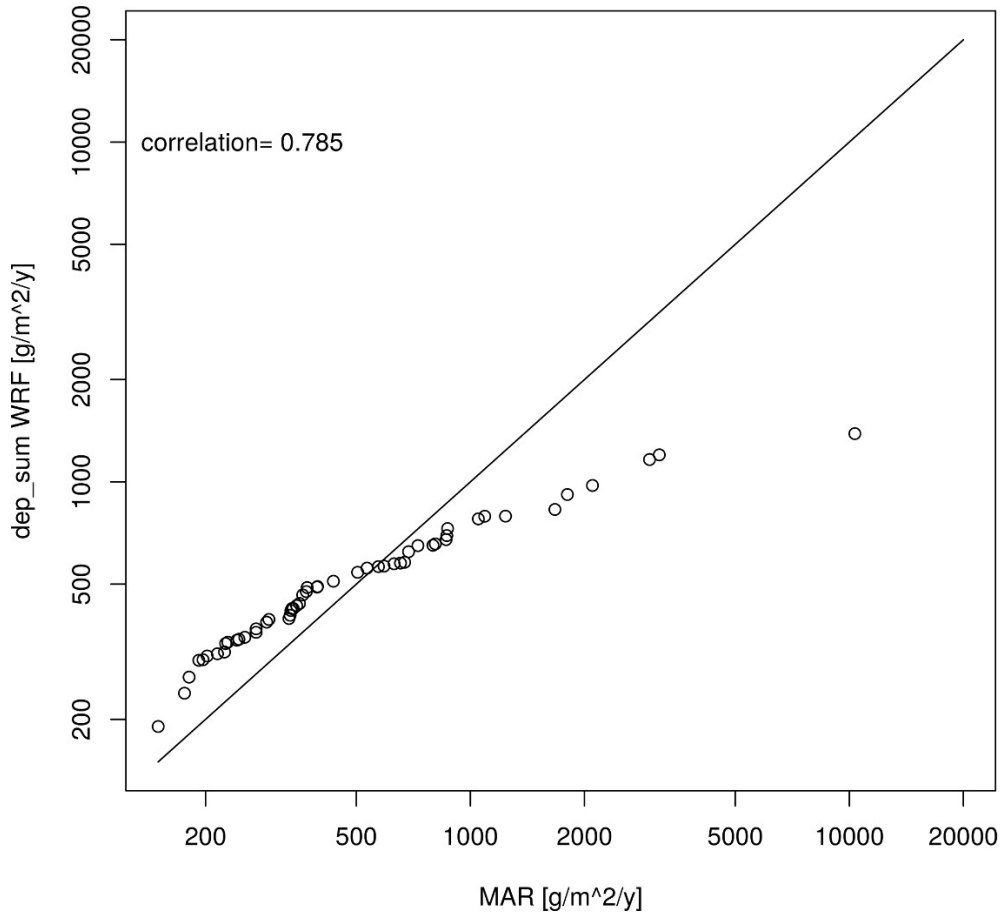


Figure 1

R1.6 Lines 268 and 278: The dimensions should be g/m<sup>2</sup>/yr and not kg/m<sup>2</sup>/yr, I guess.

A Thanks for this comment. In the new version, this is corrected.

R1.7 Lines 297-298: State clearly if this is bulk or dust MAR.

A "The largest dust deposition rates during the LGM occurred [...]" refers to the WRF-Chem-LGM simulations. Any other wording would be inconsistent with all other sections of the manuscript. A further distinction between WRF-Chem-LGM particles up to 12 microns and up to 20 microns is not necessary here, since this sentence applies to both deposition rates (based on 12 and 20 micron). If we had referred to results from fieldwork, we would have used the terms MAR (or MAR10) instead.

## Technical corrections

R1.8 Line 29: Ujvari et al (2012) is not listed in "References"; is this the cited study of the authors from 2017?

A Due to a UTF-8 sorting error, it is listed at the end of the References list. Thanks for pointing to this. In the new version, the References list is re-sorted.

R1.9 Line 42: Ujvari et al. (2010) cannot be found in the reference list

A Thanks for pointing to this; in the new version, this is corrected.

R1.10 Line 133: missing full stop at the end of sentence

A Thanks for pointing to this; in the new version, this is corrected.

R1.11 Line 249: write "average dust emission"

A Thanks for pointing to this; in the new version, this is corrected.

# Referee#2

Interactive comment on

“Linkage between Dust Cycle and Loess of the Last Glacial Maximum in Europe”

by Erik Jan Schaffernicht et al.

Anonymous Referee #2

Manuscript number: acp-2019-693

R= Referee#2

A= Authors' reply

R:

This paper examines the contribution of mineral dust cycle to loess deposits in Europe during the Last Glacial Maximum (LGM) using the output from the Max-Planck-Institute Earth System Model (MPI-ESM) and simulations from the WRF-Chem model. The simulated dust deposition rates are largely consistent with site records of mass accumulation rates of the loess deposits. Using statistic dynamical downscaling, it is found that the east sector and cyclonic winds are the dominant circulation regimes during the LGM and thus result in a westward dust transport to the central and eastern Europe. The seasonal variations in dust emission and deposition are also analysed. Overall, the paper is well organized and written. However, in some places, the purpose of the analysis and methodology need further clarification.

A:

We thank the referee very much for the valuable comments and suggestions to improve the manuscript. Subsequently, the referee's comments are addressed point by point. It is our aim to fulfil the demands to publish this manuscript in ACP.

(Reference keys that are not fully written out in this document refer to the References section of the updated manuscript)

## Major comments

R2.1 I'd suggest adding a discussion about the motivation to use the WRF-Chem and MPI-ESM to study dust cycles during the LGM.

A The MPI-ESM was used as its 1850–2005 experiment reproduces best the recent observed wind distribution over central Europe. This result was found by comparing the CWT distribution of four different global earth system/circulation models (MPI-ESM, CCSM, MRI and MIROC) to reanalyses data for central Europe (Schaffernicht, Erik Jan: *Linkage between Dust Cycle and European Loess in the Last Glacial Maximum Determined by Atmospheric Model Simulations*.

Inaugural Dissertation, PhD thesis, University of Cologne, Germany, 2018.

<https://kups.ub.uni-koeln.de/9036/>

<http://kups.ub.uni-koeln.de/id/eprint/9036>

).

In addition, access to boundary conditions that are updated frequently enough to carry out the intended WRF-Chem-LGM experiments was only offered by the MPI-LGM.

The WRF-Chem was chosen to be the core for the LGM dust simulation model because it has already been evaluated successfully in numerous recent studies comparing its dust simulations with observations (Bian et al. 2011, Zhao et al. 2011, Zhao et al. 2012, Rizza et al. 2016, Baumann et al. 2019).

- R2.2 As mentioned in section 1, results from previous global simulations largely underestimate the mass accumulation rates (MARs) of dust depositions. Is this due to the coarse resolution of the global models...
- A Yes and due to local small scale dust sources and deposition processes (Werner et al. 2002).
- R2.3 ...or insufficiency of the dust emission schemes to capture certain processes of the dust emission and transport?....
- A Yes (Werner et al. 2002) and also a missing process or a low sensitivity in the dust model is possible (Hopcroft et al. 2015 JGRA).
- R2.4 ...Or is it related to unrealistic land surface settings for the LGM...
- A Yes: Probably due to the missing glaciogenic dust sources (Mahowald et al. 2006, Hopcroft et al 2015JGRA) and parameterizations of source regions and source material availability are undersensitive to LGM conditions (Hopcroft et al. 2015 JGRA)
- R2.5 ...or misrepresentation of the atmospheric circulation patterns in the models?
- A Yes, e.g. Ludwig et al. (2016). Lacking interannual variability and dust storm events might be another factor (Hopcroft et al. 2015 JGRA).
- Corresponding statements have been added to the manuscript.
- R2.6 Similarly, please consider adding explanation/discussion about why current work better captures the magnitude of the MARs in the result section.
- A Corresponding explanations/discussion has been added to the manuscript in the section: "Conforming Dust Deposition and Loess Accumulation Rates".
- Current work captures better the magnitude of the MARs because:
- the regional simulations are run with a much higher resolution compared to previous studies
  - its simulations include additional dust sources that likely existed due to the glacial topography.
  - it takes into account Ginoux's dust function (Ginoux et al. 2001) and resolves Europe at higher spatiotemporal resolution
  - it takes into account dynamic soil moisture, vegetation and snow cover
  - its boundaries are driven by the LGM simulation of the MPI-ESM. For the end of the 20<sup>th</sup> century, this ESM reproduced the observed atmospheric circulation over Europe better than other ESM/GCMs (Ludwig et al. 2016).
  - it uses a well-tested and observation-proofed dust emission scheme (Shao 2004)
- R2.7 The purpose of using dynamic downscaling and statistic dynamic downscaling is not quite clear, and the method of dynamic downscaling is somewhat vague. For instance, 30 years of simulations are conducted using dynamic downscaling (line 82). What time period does the simulation cover? Are the 30 years consecutive?

- A The dynamic and statistic dynamic downscaling serve to simulate the glacial dust cycle at high resolution using the WRF-Chem-LGM including seasonal and circulation weather type dependent aspects. More details are provided in the answer to R2.11.
- The MPI-LGM (simulation in equilibrium setup) covers average LGM conditions. Its arbitrary timestamp is 1919-01-01 to 1948-12-31.
- The 30 years are consecutive (see line 83 in the initial manuscript).
- R2.8 What's the setting of sea surface temperature?
- A The sea surface temperature and sea ice cover are updated daily based on the corresponding MPI-LGM variables.
- R2.9 What's the setting of vegetation cover?
- A The vegetation cover has been reconstructed from the CLIMAP LGM maximum vegetation cover and the vegetation dynamics extracted from the present-day WRF geo data. Details can be found in manuscript line 67 and Supplementary Table S2 and S3.
- R2.10 More importantly, what's the benefit of using statistic dynamic downscaling?
- A A high resolved (i.e. approximately 50 km grid spacing) reconstruction of the glacial dust cycle based on statistic dynamic downscaling requires much less computation time. It is the first proof-of-concept that statistic dynamic downscaling not only works for wind regime analyses but also for reconstructing the mineral dust cycle. Also, statistic dynamic downscaling enables analysing the dust cycle by wind regimes.
- R2.11 Why not use the results from the dynamic downscaling directly, e.g., by selecting the circulation weather types (CWTs) from the 30-year run?
- A Extracting CWT samples directly from the 30-year run would imply including a non-quantifiable amount of background dust; thus, the deposition rates extracted in this case might not solely be related to the specific CWT.
- Also, the results based on the statistic dynamic downscaling of the 100-year MPI-LGM are intended for comparison to the dynamic downscaling results that base on only 30 years. Selecting CWTs only from the 30-year run would ignore 70 years of daily records for the LGM wind field over Europe. In addition, when designing the concept for this study, there was a lack of studies showing that a dynamic climate-dust cycle downscaling over 30 years is possible within the numerical limitation of the available high performance computer (HPC). As the implementation of the statistical dynamic downscaling implied a reduction of the required simulation days by a factor of ten without missing any major wind direction feature, it is a promising approach. This finding can be important in particular for larger domains and/or models requiring much more computation time for dynamic downscaling.
- R2.12 3. Please consider adding the dust emission scheme (Shao 2004) to section 2, so the readers would have a clearer idea about how dust emission is initiated and constrained in the model. Information such as dust size bins is also needed.

- A The 0–20  $\mu\text{m}$  particle size range is partitioned in five dust size bins: 0-2, 2-3.6, 3.6-6, 6-12, 12-20  $\mu\text{m}$ . Added to the manuscript in the first paragraph of the section "Data and Methods".

The dust emission scheme (Shao 2004) is referred to in Section 2, first paragraph (e.g., in manuscript line 60): "This mode implies the application of the size-resolved University of Cologne dust emission scheme (Shao2004) [...]". The structure and implementation of this dust emission scheme is extensive and cannot be summarized in a few sentences. It consists of many physical, mathematical and numerical/technical aspects, which are discussed in detail in 'Shao (2004)'. If there is a specific detail of the emission scheme that Referee2 requires here, we kindly ask Referee2 to let us know which particular formula or detail (s)he misses here. It would go beyond the scope of this study to (re-)discuss 'Shao (2004)'. It is kindly recommended to read 'Shao (2004)' for more information on the dust emission scheme.

## Minor points

- R2.13 1. By using the CWTs as criteria to conduct statistic dynamic downscaling, it assumes that atmospheric circulation pattern is the dominant factor influencing dust deposition, other factors, such as land surface features (e.g. vegetation coverage, soil moisture), and environmental factors (e.g. wind frequency and magnitude, precipitation) play minor roles. Is this a good assumption? You may want to add some discussion in section 2 about this.

- A The deposition location(s) depend(s) on different factors, foremost the speed and direction (and thus implicitly also the emission locations) of the wind that caused emission and transport of the dust particles (Darmenova et al. 2009). This constrains the potential locations for deposition. In addition, land surface features can affect the deposition, yet, it is beyond the scope of this study to quantify their proportional effect in the WRF-Chem-LGM among other factors such as the CWTs.

The atmospheric circulation patterns are the most relevant factor for the complete dust cycle including emission, transport and deposition. They include environmental factors implicitly, e.g. the wind regime frequency and precipitation likelihood. The effects of soil moisture, snow and vegetation cover on the dust cycle emerge in particular on the seasonal scale (Fig. 9) and are taken into account by the applied dust emission scheme. The agreement between the statistic dynamic and the dynamic downscaling results demonstrates that the CWT-focused approach captures the dominant factors well. (Manuscript updated)

- R2.14 2. Instead of showing schematic of the atmospheric circulation patterns (e.g., Fig. 2), I wonder if you may add figures in text or in the supplement to show the composite of wind patterns either from the MPI-ESM or WRF-Chem simulations to better demonstrate the transport pathways of the dust.

- A The wind patterns are shown by the grey lines in Fig. 2. They were extracted directly from the WRF-Chem-LGM experiments. (The caption of Fig. 2 has been updated accordingly.)

The composite of wind patterns over Europe from the MPI-ESM can be found and has already been discussed in Ludwig et al. (2016).

R2.15 Lines 55-56, what's the setting of sea surface temperature for the WRF-Chem? Is it also from the MPI-ESM simulation?

A Yes, it is from the MPI-LGM.

R2.16 4. Lines 68-69, are the vegetation coverage data monthly or annually?

A They are monthly:

"...using the corresponding **monthly** fractions of the present-day WRF maximum vegetation cover..." (near line 69).

Based on the CLIMAP maximum LGM vegetation cover reconstruction, a monthly vegetation cover was calculated as an analog to the present-day monthly WRF vegetation dynamics

R2.17 5. Lines 85-87, CWT on what level? Near-surface, 850 hPa, or a higher level?

A CWTs are based on the mean sea level pressure; references Jones et al 1993, Jones et al 2003 are in the manuscript and provide the details (near line 85).

R2.18 6. Lines 87-88, "to compare the prevailing wind directions over Europe during the Pre-Industrial (PI) and the LGM...". Why not compare with present-day wind direction? In the abstract, "present-day prevailing westerlies" is mentioned, is it referred to the result from the PI simulation?

A The LGM CWT frequencies have also been compared with present-day CWT frequencies:

Table 2-extended:

	C	A	NE	E	SE	S	SW	W	NW	N
LGM	22.2	8.9	12.4	13.4	10.2	9.7	6.8	4.3	5.0	7.0
PI	10.6	24.1	7.9	5.2	4.9	7.6	11.6	11.1	9.4	8.3
present-day	10.6	23.9	7.3	5.1	4.7	7.5	12.4	11.4	9.2	8.0

The present-day frequencies are not shown in Table 2 for consistency. The LGM MPI-ESM experiment is an equilibrium experiment (without transient forcing). Thus, comparing it to equilibrium experiments such as for the PI is more robust because this does not induce uncertainty due to different kind of permanency of model forcing setups. Table 2-extended shows that the corresponding present-day CWT frequencies obtained from the transient MPI-ESM experiment are indeed almost identical with the PI CWT frequencies.

The manuscript is updated in section "East Sector Winds and Cyclones over Central Europe" by:

The CWT frequencies for the present (not shown) and PI are very similar, therefore it is possible to use the term present-day to refer to both the PI and the actual present-day frequencies.

R2.19 7. Line 89, what's the difference between the MPI-LGM run and MPI-ESM-P run? How long are these simulations?

A The MPI-ESM-P is a typo. The sentence in line 89 (Data and Methods, paragraph 4) is now updated. The MPI-LGM is 100 years long.

R2.20 8. Line 90, why is this point selected? Is it the center of the Loess?

A Yes, approximately; taking into account that the present-day loess sites exist for example in northwestern France and also in Ukraine. Also, it (17.5°E, 47.5°N) is located near the Carpathian basin which is a prominent loess region.

R2.21 9. Line 94, what are the differences in 13 simulations? Initial conditions?

A Yes, the 13 simulations differ slightly in their initial and boundary conditions.

R2.22 10. Line 96, what is the definition of a "CWT set"? 8 consecutive days with the same CWT? Can you please list the number of CWT sets from the MPI-ESM simulation?

A A CWT set consists of 8 consecutive days. At least the CWT of the third, fourth and fifth day of these 8 consecutive days (also called "the 3 main days", cf. Table 1) must be identical to the requested CWT. For most of the 13 simulations, all of their eight consecutive days belong to the same CWT.

130 CWT sets have been chosen from the MPI-LGM. (cf. near line 94)

R2.23 11. Fig. 1, can you please add the location of the Loess to the figure?

A Fig. 1 focuses on the numerical WRF-Chem-LGM setup (i.e. the model input data) and it contains already the dotted area that shows that all areas outside this area are excluded from being a potential dust source. It would overload this map with too many colours, shades, lines and symbols if we add more independent data sets that need to be clearly distinguishable without affecting the already shown layers. Adding these loess locations would also suggest that they were used as input data for the WRF-Chem-LGM experiments. This would be misleading because the loess sites samples are only used to compare the WRF-Chem-LGM results to. They are not part of any simulation.

R2.24 12. Can you please add some explanation about Table 1? e.g., what's heterogeneous sequence? Why are spin-up records preferred?

A Table 1:

Each CWT sequence consists of 8 consecutive days, i.e. 2 spin-up, 3 main and 3 tracking days. In all CWT sequences, the CWT of the 3 main days is identical and defines the desired CWT for the whole 8-day episode.

For rare cases for which no 13 distinct 8-day samples for the same CWT were available in the MPI-LGM, the strict selection criteria has been weakened. That is, the 2 spin-up days are then allowed to be samples of a different CWT. If applying this weakened selection criteria was still insufficient to extract 13 different 8-day episodes from the MPI-LGM, then the selection criteria was weakened further, that is, also the 3 tracking days are allowed to deviate from the CWT of the main days.

This approach implies that the priority of the 3 tracking days to fit to the CWT of the main days is higher (++) than that of the 2 spin-up days (+).

An episode is called *heterogeneous* if at least 1 (out of 5 possible) record differs from the desired CWT of the episode's main days.

The caption of Table1 has been updated.

R2.25 13. Line 135, why do you mention Fig. 9a here?

A Fig. 9a is mentioned here since it shows the importance of east sector winds.

R2.26 14. Line 181, why do you select 12 and 20  $\mu\text{m}$ ?

Is 20  $\mu\text{m}$  the largest dust size bin in the model?

The results from FD12 in Fig. 4 seem not discussed in section 3.4.

A 20  $\mu\text{m}$  is selected because it is the upper limit of particle sizes included in the WRF-Chem-LGM with the applied dust emission scheme.

12  $\mu\text{m}$  is selected because the WRF-Chem-LGM particle size bin distribution provides this limit as the nearest approximation of the deposition values for 10  $\mu\text{m}$  particle size limit that are commonly published in studies based on mass accumulation rates (MAR10 = MAR 10  $\mu\text{m}$ ) from loess fieldwork samples.

Yes, 20  $\mu\text{m}$  is the largest dust size bin in the model. (Manuscript updated)

R2.27 15. Line 214, add "(Fig. 7)" after "vegetation cover".

A Thanks for this comment. In the new version, this is corrected. We assume Referee2 refers to line 213 as "veg. cover" does not occur in line 214.

R2.28 16. Can you please add the location of dust source (as displayed in Fig. 1) to Fig. 6?

A Parts of Fig. 1 and Fig. 6 are possibly misunderstood:

Fig. 1 does not show any dust source location. Instead, the dotted area limits the area for **potential** dust sources. That is, it rather excludes regions (i.e. the non-dotted) as potential dust sources since they have a very low or zero potential erodibility according to Ginoux's time-independent dust function (Ginoux et al. 2001). If the dotted regions eventually become dust sources depends on additional dynamic factors such as e.g. the atmospheric circulation (in particular the wind speed) and surface conditions (e.g. snow and vegetation cover, soil moisture). As Fig. 6 displays seasonal dust cycle aspects, it should be noted, that (in addition to the before mentioned) the dotted area results from spatiotemporal average (i.e. annual) LGM conditions. It does not take into account (nor adapt to) the seasonal changes that occurred during the LGM.

Fig. 6 focuses on the seasonal dust deposition rates. Adding Ginoux's time-independent potential erodibility mask (shown in Fig. 1) would suggest that this mask is adjusted to seasonal differences and particularly appropriate for seasons. Yet, this suggestion is misleading and would create a misleading understanding of the Fig.6 for the reader.

Nevertheless, the referee's request is already met in Fig. 5, which shows the location of the dust sources resolved by season. In addition, Fig. 5 shows the seasonal dust emission rates of the dust sources.

For clarity and readability, it is suggested to **not** add further colours, shapes, contours nor shades to Fig. 6. Otherwise, it would become overloaded.

# Linkage between Dust Cycle and Loess of the Last Glacial Maximum in Europe

Erik J. Schaffernicht<sup>1</sup>, Patrick Ludwig<sup>2</sup>, and Yaping Shao<sup>1</sup>

<sup>1</sup>Institute for Geophysics and Meteorology, University of Cologne, 50969 Köln, Germany

<sup>2</sup>Institute for Meteorology and Climate Research, Karlsruhe Institute of Technology, 76131 Karlsruhe, Germany

**Correspondence:** Erik J. Schaffernicht (eschaffe@uni-koeln.de)

**Abstract.** This article establishes a linkage between the mineral dust cycle and loess deposits during the Last Glacial Maximum (LGM) in Europe. To this aim, we simulate the LGM dust cycle at high resolution using a regional climate-dust model. The model-simulated dust deposition rates are found to be comparable with the mass accumulation rates of the loess deposits determined from more than 70 sites. In contrast to the present-day prevailing westerlies, winds from northeast, east and southeast (36%) and cyclonic regimes (22%) were found to prevail over central Europe during the LGM. This supports the hypothesis that the recurring east sector winds associated with a high-pressure system over the Eurasian ice sheet (EIS) dominated the dust transport from the EIS margins in eastern and central Europe. The highest dust emission rates in Europe occurred in summer and autumn. Almost all dust was emitted from the zone between the Alps, the Black Sea and the southern EIS margin. Within this zone, the highest emission rates were located near the southernmost EIS margins corresponding to the present-day German-Polish border region. Coherent with the persistent easterlies, westwards running dust plumes resulted in high deposition rates in western Poland, northern Czechia, the Netherlands, the southern North Sea region and on the North German Plain including adjacent regions in central Germany. The agreement between the climate model simulations and the mass accumulation rates of the loess deposits corroborates the proposed LGM dust cycle hypothesis for Europe.

## 1 Introduction

The Last Glacial Maximum (LGM,  $21\,000 \pm 3\,000$  yr ago) is a milestone in the Earth's climate, marking the transition from the Pleistocene to the Holocene (Clark et al., 2009; Hughes et al., 2015). During the LGM, Europe was dustier, colder, windier and less vegetated than today (Újvári et al., 2017). The polar front and the westerlies were located at lower latitudes associated with a significant increase in dryness in central and eastern Europe (COHMAP Members, 1988; Peyron et al., 1998; Florineth and Schlüchter, 2000; Laîné et al., 2009; Heyman et al., 2013; Ludwig et al., 2017). The formation of the Eurasian ice sheet (EIS, Fig. 1 and 2) synchronized with a sea level lowering of between 127.5 m and 135 m (Yokoyama et al., 2000; Clark and Mix, 2002; Clark et al., 2009; Austermann et al., 2013; Lambeck et al., 2014). It led to different regional circulation patterns over Europe (Ludwig et al., 2016). The greenhouse gas concentrations (185 ppmv CO<sub>2</sub>, 360 ppbv CH<sub>4</sub>) were less than half compared to today (Monnin et al., 2001) providing more favorable conditions for C<sub>4</sub> than C<sub>3</sub> plants. This led to more open vegetation (Prentice and Harrison, 2009; Bartlein et al., 2011) such as grassland, steppe, shrub and herbaceous tundra (Kaplan

et al., 2003; Ugan and Byers, 2007; Gasse et al., 2011; Shao et al., 2018). Central and eastern Europe were partly covered by  
26 taiga, cold steppe or montane woodland containing isolated pockets of temperate trees (Willis and van Andel, 2004; Fitzsim-  
mons et al., 2012). Polar deserts characterized the unglaciated areas in England, Belgium, Denmark, Germany, northern France,  
28 western Poland and the Netherlands (Ugan and Byers, 2007). These land surfaces and biome types favored more dust storms  
and transport over Europe (Újvári et al., 2012).

30 Loess as a paleoclimate proxy provides one of the most complete continental records for characterizing climate change and  
evaluating paleoclimate simulations (Singhvi et al., 2001; Haase et al., 2007; Fitzsimmons et al., 2012; Varga et al., 2012).  
32 In Europe, loess covers large areas with major deposits centered around 50°N (Antoine et al., 2009b; Sima et al., 2013).  
However, although numerous European loess sequences date to the LGM, it is not well understood where the dust originated  
34 that contributed to the loess formation (Fitzsimmons et al., 2012; Újvári et al., 2017). There are various hypotheses for the  
potential dust sources, yet they are not fully tested because the dust cycle of the LGM is neither well understood nor quantified.  
36 The use of loess as a proxy for paleoclimate reconstruction is considerably compromised because the linkage between the loess  
deposits and the responsible physical processes is unclear (Újvári et al., 2017). Reliable paleodust modeling is a promising way  
38 to establish this linkage and strengthen the physical basis for paleoclimate reconstructions using loess records. Such attempts  
have been made for example by Antoine et al. (2009b), who analyzed the Nussloch record. They suggested that rapid and  
40 cyclic aeolian deposition due to cyclones played a major role in the European loess formation during the LGM.

However, significant discrepancies exist between the mass accumulation rates (MARs) of aeolian deposits that are esti-  
42 mated from fieldwork samples and the dust deposition rates calculated by climate model simulations (Újvári et al., 2010):  
For Europe, the global LGM simulations ~~calculate result in~~ dust deposition rates (based on different particle size ranges)  
44 of less than  $100 \text{ g m}^{-2} \text{ yr}^{-1}$  (Werner, 2002; Mahowald et al., 2006; Hopcroft et al., 2015; Sudarchikova et al., 2015; Al-  
bani et al., 2016). These are substantially smaller than the MARs (on average:  $800 \text{ g m}^{-2} \text{ yr}^{-1}$ ) that have been reconstructed  
46 from more than 70 different loess sites across Europe (Supplementary Table S1). This underestimation is probably due to the  
coarse resolution of the global models which ignores dust sources, emission, transport and deposition processes at the small  
48 scale (Werner, 2002). Other causes can be missing glaciogenic dust sources, a low dust model sensitivity, an underestimated  
source material availability (Mahowald et al., 2006; Hopcroft et al., 2015), a biased atmospheric circulation, and a lack of dust  
50 storms and interannual variability (Hopcroft et al., 2015; Ludwig et al., 2016).

For this study, we simulated the aeolian dust cycle in Europe using a LGM-adapted version of the Weather Research and  
52 Forecasting Model coupled with Chemistry (Klose, pers. comm.; Grell et al., 2005; Fast et al., 2006; Kang et al., 2011; Ku-  
mar et al., 2014; Su and Fung, 2015) referred to as the WRF-Chem-LGM. ~~Along with its climate modeling capacity, the~~  
54 The boundary conditions for the WRF-Chem-LGM ~~can well represent the~~ simulations are provided by the LGM simulation  
(MPI-LGM) of the Max-Planck-Institute Earth System Model (MPI-ESM; Jungclaus et al., 2012, 2013; Giorgetta et al., 2013;  
56 Stevens et al., 2013). This model was chosen since its 1850–2005 experiment reproduces best the recent observed wind  
distribution over Europe compared to the other climate models (Ludwig et al., 2016). In addition, the MPI-LGM provides three  
58 dimensional boundary conditions updated frequently enough to carry out the intended WRF-Chem-LGM experiments. The  
WRF-Chem was chosen since it has already been evaluated successfully in many recent studies comparing its dust simulations

60 [with observations \(Bian et al., 2011; Kang et al., 2011; Zhao et al., 2011, 2012; Rizza et al., 2016; Baumann-Stanzer et al., 2019\)](#)  
61 [. Therefore, it is likely that the newly created WRF-Chem-LGM will simulate the LGM dust emission, transport, and deposi-](#)  
62 [tion processes. This model capacity similarly well. This capacity of the WRF-Chem-LGM](#) allows reducing the discrepancies  
63 between the MARs and the simulation-based ~~calculated~~ dust deposition rates. It enables the establishment of a linkage between  
64 the glacial dust cycle and the [on site](#) loess deposits.

## 2 Data and Methods

65 The WRF-Chem-LGM consists of fully coupled modules for the atmosphere, land surface, and air chemistry. The simulation  
66 domain encompasses the European continent including western Russia and most of the Mediterranean (Fig. 1) discretized  
67 by a grid spacing of 50 km and 35 atmospheric layers. The domain boundary conditions were 6-hourly updated by using  
68 the ~~LGM simulation (MPI-LGM) of MPI-LGM. The sea surface temperature and sea ice cover are updated daily based~~  
69 [on the corresponding MPI-LGM variables.](#) To simulate the dust cycle including dust emission, transport and deposition, the  
70 dust-only mode of the WRF-Chem-LGM was selected. This mode implies the application of the size-resolved ([dust size](#)  
71 [bins: 0–2, 2–3.6, 3.6–6, 6–12 and 12–20 μm](#)) University of Cologne dust emission scheme (Shao, 2004), the Global Ozone  
72 Chemistry Aerosol Radiation Transport (~~GOCART; Chin et al., 2000~~)(GOCART; Chin et al., 2000; Ginoux et al., 2001;  
73 Chin et al., 2002; Ginoux et al., 2004), the dry (~~Wesely, 1989~~) and the wet deposition ~~module (Jung et al., 2005)~~[modules](#)  
74 ([Wesely, 1989; Chin et al., 2002; Grell et al., 2005; Jung et al., 2005](#)).

75 To replace the present-day WRF surface boundary conditions by the LGM conditions, the data sets for the global 1° resolved  
76 land-sea mask and the topography offset provided by PMIP3 (Paleoclimate Model Intercomparison Project Phase 3; Braconnot  
77 et al., 2012) were interpolated to the 50 km grid (Fig. 1, Supplementary Table S2 and S3). To represent the LGM glaciers and  
78 land use, the 2° CLIMAP reconstructions (Climate: Long range Investigation, Mapping, and Prediction; Cline et al., 1984)  
79 were also interpolated to the 50 km grid and converted (Ludwig et al., 2017) to the WRF-compatible United States Geologi-  
80 cal Survey categories (USGS-24) to replace their present-day analogs. The relative vegetation seasonality during the LGM is  
81 assumed to resemble to the present. Based on this uniformitarianism approach, the CLIMAP maximum LGM vegetation cover  
82 reconstruction (Cline et al., 1984) was weighted using the corresponding monthly fractions of the present-day WRF maximum  
83 vegetation cover and prescribed in the model.

The erodibility at point  $p$  during the LGM is approximated by

$$86 \quad S = \left( \frac{z_{\max} - z}{z_{\max} - z_{\min}} \right)^5 \quad (1)$$

with  $z$  being the LGM terrain height at  $p$  and  $z_{\min}$  ( $z_{\max}$ ) representing the minimal (maximal) height in the  $10^\circ \times 10^\circ$  area  
87 centered around  $p$  (Ginoux et al., 2001). Setting  $S$  to zero where the CLIMAP bare soil fraction reconstruction is less than  
88 0.5 refines this approximation. The adapted University of Cologne dust emissions scheme takes into account that the erodi-  
89 bility exceeds a lower limit of 0.09 for emission to occur. This suppresses dust sources in areas that had been attributed small

physically meaningless interpolation-caused erodibility artifacts. The vegetation and snow cover are considered mutually independent and uniformly distributed within a grid cell, i.e. the erodible area is multiplied by the fractional factor  $(1 - c_{\text{snow}})$  to account for snow cover.

To simulate the LGM dust cycle with the WRF-Chem-LGM, two downscaling approaches of the MPI-LGM were implemented: the dynamic downscaling approach and the statistic dynamic downscaling approach. Both emerge from simulations that base on identically configured numerical schemes representing the atmospheric chemistry and physics in the WRF-Chem-LGM. Using dynamic downscaling, a consecutive 30 year simulation (corresponding to more than 10 000 days) was performed. In contrast, the statistic dynamic downscaling is based on 130 mutually independent episodes each spanning eight days, or a total of 1040 days. The episode selection relies on the Circulation Weather Type (CWT) classification (Jones et al., 1993, 2013; Meyers et al., 2014; Ludwig et al., 2016) of the MPI-LGM records into ten classes: Cyclonic, Anticyclonic, Northeast, East, Southeast, South, Southwest, West, Northwest and North. The CWT classification approach is chosen since the atmospheric circulation patterns are the dominant factor for controlling dust emission from and deposition on dry, low and sparsely vegetated soil surfaces (Ginoux et al., 2001; Darnenova et al., 2009; Shao et al., 2011a, b). Such kind of surfaces characterized the unglaciated regions in central and eastern Europe during the LGM (Ugan and Byers, 2007). To compare the prevailing wind directions over Europe during the Pre-Industrial (PI) and the LGM, the daily mean sea level pressure patterns (interpolated to 2.5° horizontal grid spacing) of the MPI-LGM and the MPI-ESM-P-MPI-ESM simulation for the PI (MPI-PI) were classified for the region centering around (17.5°E, 47.5°N). For records showing rotational and directional CWT patterns, only the directional pattern is counted. By counting and statistically evaluating the CWTs of all records, a LGM and a PI CWT occurrence frequency distribution is established. The LGM distribution served to reconstruct the LGM dust cycle using statistic dynamic downscaling. It also enabled analyzing the contributions of each wind regime to the dust cycle.

For the statistic dynamic downscaling, we performed 130 WRF-Chem-LGM simulations in total, i.e. 13 simulations for each of the 10 CWT classes. For each of these eight-day spanning simulations, independent consecutive sequences of boundary conditions were chosen out of all MPI-LGM records of the same CWT class. For CWTs with too few sets of distinct consecutive MPI-LGM records of the required CWT, the remaining sets were chosen applying less strict selection criteria (Table 1). For the analysis of all performed episodic simulations, the first two days of each episode are considered as spin-up days and excluded. The reconstruction of quantity  $Q$  using statistic dynamic downscaling is then calculated from the weighted ensemble mean (Reyers et al., 2014):

$$\langle Q \rangle = \sum_i \frac{f_i}{T} \int_T Q(t) dt \quad (2)$$

with  $i$  representing the  $i^{\text{th}}$  CWT,  $f_i$  its occurrence frequency and  $T$  its duration. To evaluate the simulations, the obtained dust deposition rates are compared to more than 70 independent MARs reconstructed from loess sites located in the simulation domain (Supplementary Table S1).

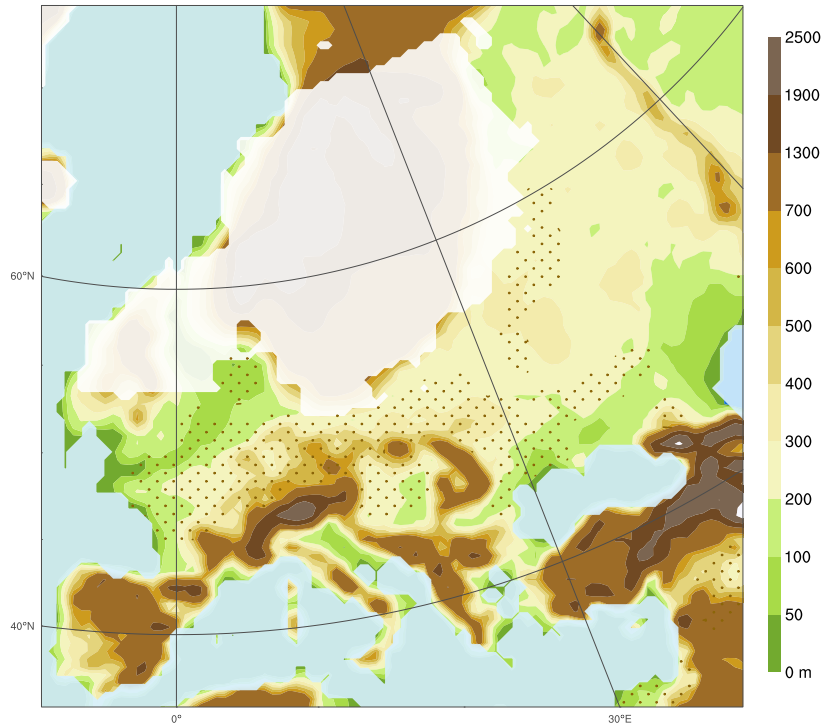


**Figure 1.** Simulation domain showing the applied topography (shaded), the potential dust source areas (dots) and the Eurasian ice sheet extent (white overlay, adapted from Cline et al., 1984) of the Last Glacial Maximum.

**Table 1.** Temporal concept for the episodic eight-day WRF-Chem-LGM simulations performed to reconstruct the LGM dust cycle based on statistic dynamic downscaling. As the MPI-LGM contains for a few CWTs less than 13 separate eight-day record sequences, some of the episodes were driven by a heterogeneous sequence of records. For That is, one (or more) of the selection records in these sequences differs in its CWT from the CWT of the records for the main days. For selecting heterogeneous sequences, the CWT-correspondence between the main and tracking records is considered of higher priority ( $\pm\pm = ++$ ) than ~~that~~ between main and spin-up records ( $\pm = +$ ).

	Days	Preferences for selecting record series from the MPI-LGM
Spin-up	2	Prefer <sup>+</sup> <u>series sequences</u> whose spin-up records have the same CWT as the main records
↓		
Main	3	All records <del>foreing that drive</del> the main part <u>(central 3 days) of each episode must be of an episode are of</u> the same CWT
↓		
Tracking	3	Prefer <sup>++</sup> <u>series sequences</u> whose tracking records have the same CWT as the main records

### 3.1 Dust Cycle Hypothesis

124 In line with previous modeling (COHMAP Members, 1988; Ludwig et al., 2016) and fieldwork studies (Dietrich and Seelos,  
 126 2010; Krauß et al., 2016; Römer et al., 2016), we hypothesize that east sector winds (i.e. northeasters, easterlies and southeast-  
 128 ers) dominated the mineral dust cycle over central Europe during the LGM (Fig. 2). This hypothesis also implies a linkage of  
 dust sources in central and eastern Europe during the LGM and the loess deposits in Europe. It is suggested here that a greater  
 130 proportion of all LGM dust deposits in central and eastern Europe comes more from sources in central and eastern Europe  
 than from sources in the Channel. The east sector winds likely contributed substantially to the formation of the European loess  
 132 belt in central Europe. Among them, the northeasters and easterlies originated most likely from dry winds that flowed down  
 the slopes of the southern and eastern EIS margins where they picked up and turned gradually into northeasters and easter-  
 lies. By blowing over the bare proglacial EIS areas, they generated dust emissions, carried the dust westwards implying dust  
 depositions in areas west of the respective dust sources.

### 134 3.2 East Sector Winds and Cyclones over Central Europe

In agreement with this hypothesis, glacial simulations for 90 ka ago evidenced katabatic winds over the EIS (Krinner et al.,  
 136 2004) and GCM simulations for the LGM indicate prevailing east sector winds over central and eastern Europe (COHMAP  
 Members, 1988; Ludwig et al., 2016). In Germany, several aeolian sediment records that are dated to the LGM originated  
 138 from more eastern sources (Dietrich and Seelos, 2010; Krauß et al., 2016; Römer et al., 2016). The CWT frequencies for the  
 present (not shown) and the PI are very similar, therefore it is possible to use the term present-day to refer to both the PI and  
 140 the actual present-day frequencies. In contrast to the dominant present-day anticyclones and west sector winds (southwesters,  
 westerlies and northwesters), east sector winds (36%) and cyclones (22%) prevailed over central Europe during the LGM  
 142 (Table 2). ~~These~~ The east sector winds are associated with a strong EIS-High (Fig. 2a and COHMAP Members, 1988). ~~This  
 finding~~ The increased frequency of cyclones over central Europe is consistent with the analysis of the LGM storm tracks ~~that  
 144 , which~~ deviated from their present-day course (Hofer et al., 2012), running either along central Europe, the Mediterranean  
 or the Nordic Seas (Florineth and Schlüchter, 2000; Luetscher et al., 2015; Ludwig et al., 2016). Their Mediterranean course  
 146 is consistent with the Alpine, western, and southern European climate proxies (Luetscher et al., 2015). In addition, the prox-  
 ies indicate a storm track branch split-off over the Adriatic that ran past the Eastern Alps to central Europe (Florineth and  
 148 Schlüchter, 2000; Luetscher et al., 2015; Újvári et al., 2017). These proxy-based findings are in line with the more frequent  
 cyclones in central Europe during the LGM (Table 2). This, in turn, can be related to the stronger and southwards shifted  
 150 jet stream (Luetscher et al., 2015; Ludwig et al., 2016) and the missing Scandinavian cyclone tracks, which were deflected  
 southwards by the blocking EIS-High. As a result, their frequency increased over central Europe (Table 2), consistent with  
 152 susceptibility- and grain-size-based results that suggest more frequent storms over western Europe. The east sector winds,  
 which more than doubled in frequency in comparison to today (36% compared to 17%, Table 2) need to be incorporated to  
 154 establish a more complete understanding of the main drivers of the dust cycle in Europe during the LGM (Fig. 9a). These

winds are also evidenced by northern-central European grain-size records for the Late Pleniglacial (Bokhorst et al., 2011).  
156 Sediment layers attributed to east wind dated to 36–18 ka BP are abundant in the Dehner Maar sediments (Eifel, Germany,  
6.5°E, 50.3°N; Dietrich and Seelos, 2010). Their provenance showed that up to every fifth dust storm over the Eifel came from  
158 the east (Dietrich and Seelos, 2010).

Our findings are in agreement with fieldwork-based results of Römer et al. (2016), who found evidence for strong east sector  
160 winds over northern, central and western Germany for 23 to 20 ka ago. Also loess in the Harz Foreland indicates a shift to  
prevailing east sector winds for the LGM (Krauß et al., 2016). The location of aeolian ridges along rivers in northeastern  
162 Belgium and a core transect near Leuven also support our finding by evidencing northeasters for the Late Pleniglacial (Renssen  
et al., 2007). In addition, northerlies, northeasters and easterlies were inferred from loess deposits west of the Maas (Renssen  
164 et al., 2007). Also for Denmark, wind-polished boulders evidence dominant easterlies and southeasters in the period of 22 to  
17 ka ago (Renssen et al., 2007). The CWT frequency distribution for the LGM (Table 2) contradicts the finding (Renssen et al.,  
166 2007) of prevailing west sector winds during the LGM in central Europe (0–30°E, 40–55°N). The distribution also contrasts  
with the finding (Sima et al., 2013) of prevailing winds from west-northwest in eastern central Europe, in particular for the area  
168 around Stayky (31°E, 50°N). More precisely, the CWT-W and CWT-NW regimes occurred in eastern central Europe in sum  
for less than 10% of the times during the LGM (Table 2), which is even less than the expectation value for a single weather  
170 type in case of a uniform CWT frequency distribution. On the contrary, the significant role of the east sector winds (Table 2)  
is consistent with the deposits on the west bank of the Dnieper (Sima et al., 2013), which are also the loess deposits closest to  
172 Stayky. In addition, sandy soil texture and sand dunes indicate prevailing northerlies and northeasters over Dobrudja (28.18°E,  
44.32°N), the eastern Walachian Plain (both located in Romania) and Stary Kaydaky (Ukraine, 35.12°E, 48.37°N; Buggle  
174 et al., 2008). The northerlies over Ukraine originated from katabatic winds descending from the EIS (Buggle et al., 2008). The  
high aridity and grain size variations of the Surduk and Stari Bezradychy records (Serbia/Ukraine, Supplementary Table S1)  
176 evidence prevailing dry and periodically strong east sector winds (Antoine et al., 2009a; Bokhorst et al., 2011).

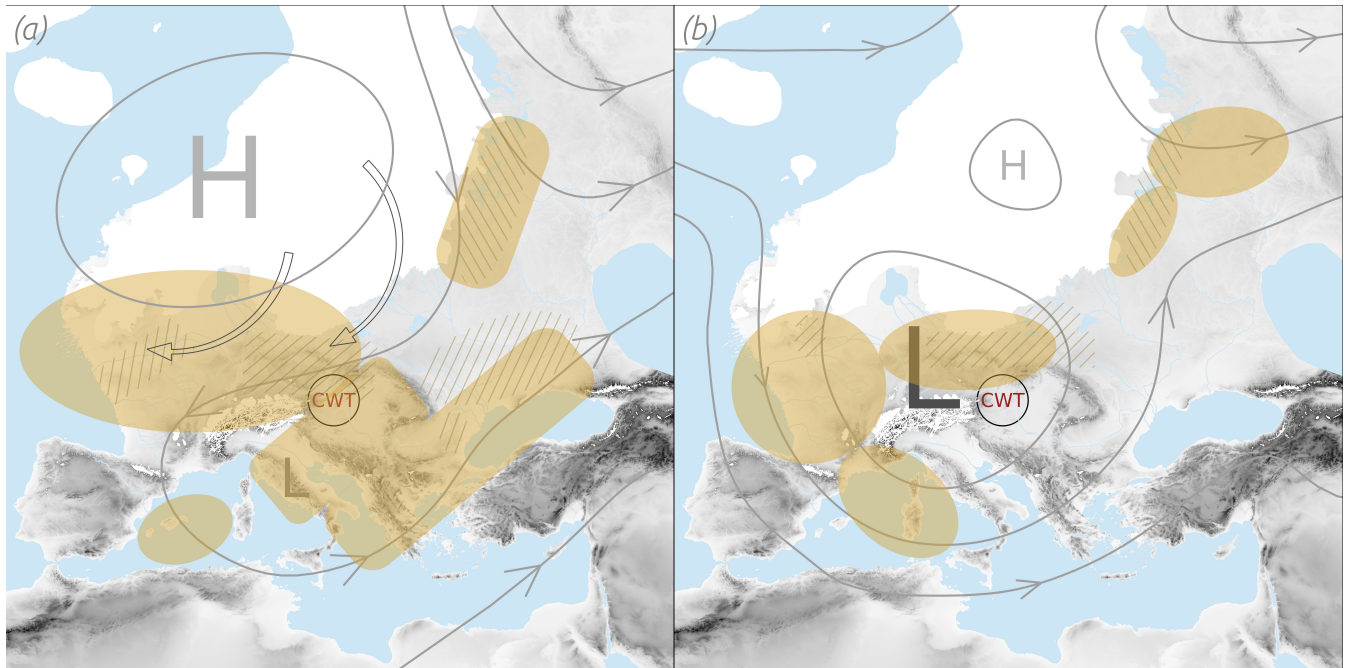


**Figure 2.** Conceptual model explaining the linkage between the European dust cycle during the Last Glacial Maximum and the loess deposits. The main dust deposition areas (filled), emission areas (hatched), [wind \(grey lines\)](#) and pressure patterns (H/L: high/low pressure) are highlighted; [all of them result from the WRF-Chem-LGM experiments](#). The center of the region for the Circulation Weather Type analysis is denoted with CWT. (a) Northeasters, easterlies and southeasters (the east sector winds; transparent arrows with black perimeter) caused by the semi-permanent high-pressure over the Eurasian ice sheet (white) prevailed 36% of the time over central Europe (Table 2). (b) The cyclonic weather type regimes which prevailed 22% of the time over central Europe (Table 2).

**Table 2.** Circulation Weather Type occurrence frequencies (%) for central Europe (centered at 17.5°E and 47.5°N) during the LGM and the Pre-Industrial period (PI). The frequencies are based on the LGM and the PI simulation of the Max-Planck-Institute Earth System Model. The Circulation Weather Type classes are: Cyclonic (C), Anticyclonic (A), Northeast (NE), East (E) followed by the remaining standard wind directions.

	C	A	NE	E	SE	S	SW	W	NW	N
LGM	22.2	8.9	12.4	13.4	10.2	9.7	6.8	4.3	5.0	7.0
PI	10.6	24.1	7.3	5.2	4.9	7.6	11.6	11.1	9.4	8.3

### 3.3 Dust Emissions from the Eurasian ice sheet margin

178 The model-simulated dust emission (Fig. 3) indicates that most dust in Europe was emitted from the less elevated corridor  
between the Alps, the Black Sea and the EIS (45–55°N). This finding is consistent with loess-based dust-flux estimates (Újvári  
180 et al., 2010). The highest emission rates ( $>10^5 \text{ g m}^{-2} \text{ yr}^{-1}$ ) occurred along the southern EIS margin (15–18°E, 51–53°N, Fig. 3).  
This location is in line with the location of the highest emissions found in the Greenland stadial GCM simulation of Sima et al.  
182 (2013), yet, our simulation indicates a larger upper limit for the emission rates ( $1000 \text{ g m}^{-2} \text{ yr}^{-1}$ ). Our results also show high  
emissions in the dry-fallen Channel and the German Bight (Fig. 3). For the latter, they compare well with a glacial climate  
184 simulation that calculated an average emission of 140 and a maximal emission of  $>200 \text{ g m}^{-2} \text{ yr}^{-1}$  (Sima et al., 2009).

The loess deposits (Újvári et al., 2010) and the model results are consistent in that the Carpathian Basin was both a dust  
186 source and a dust sink (Fig. 3 and 4). Major dust sources surrounding the Carpathians and the Eastern Alps (Fig. 3) are in  
line with deposits in Serbia and the Carpathian Basin (Újvári et al., 2010; Bokhorst et al., 2011). The dust emissions from  
188 the Lower Danube Basin (Fig. 3) are in agreement with plentiful sediment supply, strong winds and dry conditions inferred  
from the plateau loess in Urluia, located near the Black Sea in southeastern Romania (Fitzsimmons and Hambach, 2014).  
190 Also the emissions from the western Black Sea littoral (Fig. 3) are consistent with provenance analyses of Eastern Dobrogea  
loess in the Lower Danube Basin (Jipa, 2014). Our results indicate a close relationship between strong dust emissions and  
192 low terrains (or basins). This relationship is found for the North Sea Basin and the European plains bordering the EIS, the  
Caucasus, the Carpathians or the Massif Central (Fig. 1 and 3). The dust emissions from the EIS margin and from the foothills  
194 of the European mountains (Fig. 3) are consistent with the loess-based finding of significant aeolian dust contributions from  
glaciogenic and orogenic dust sources (Újvári et al., 2010).

### 196 3.4 Conforming Dust Deposition and Loess Accumulation Rates

~~The European loess belt (Kukla, 1977; Little et al., 2002; Haase et al., 2007; Sima et al., 2009) is the key to validating paleo  
198 climate dust simulations for Europe. It corresponds to the unglaciated European area that was bounded northwards by the  
EIS and southwards by the Alps, the Dinaric Alps and the Black Sea. Compared to the GCM-based dust simulations, our  
200 simulated dust deposition rates (Compared with the GCMs (Werner, 2002; Mahowald et al., 2006; Hopcroft et al., 2015;  
Sudarchikova et al., 2015; Albani et al., 2016), the WRF-Chem-LGM dust deposition rates ( $F_D$ ; Fig. 4) reproduce the MARs  
202 (Supplementary Table S1, Fig. 4a and b) and MAR10 (Supplementary Table S1, Fig. 4c and d) better, at least by one order  
of magnitude. One factor for this improvement is most likely the higher spatiotemporal resolution (Ludwig et al., 2019) of the  
204 WRF-Chem-LGM experiments combined with the provided higher resolved geographical input data, for example the regional  
LGM topography, land use and dynamic (yet monthly prescribed) vegetation cover. The boundary conditions provided by the  
206 MPI-LGM could also be a factor for this improvement. Taking into account that the MPI-ESM experiment for the present  
reproduces the observed atmospheric circulation over Europe better than other GCMs (Ludwig et al., 2016), it is likely that  
208 MPI-LGM also reproduces the LGM conditions more realistically. Another factor could be the orography-based estimated  
fraction of alluvium (Ginoux et al., 2001) combined with the proxy-based reconstructed bare soil fraction (Cline et al., 1984).~~

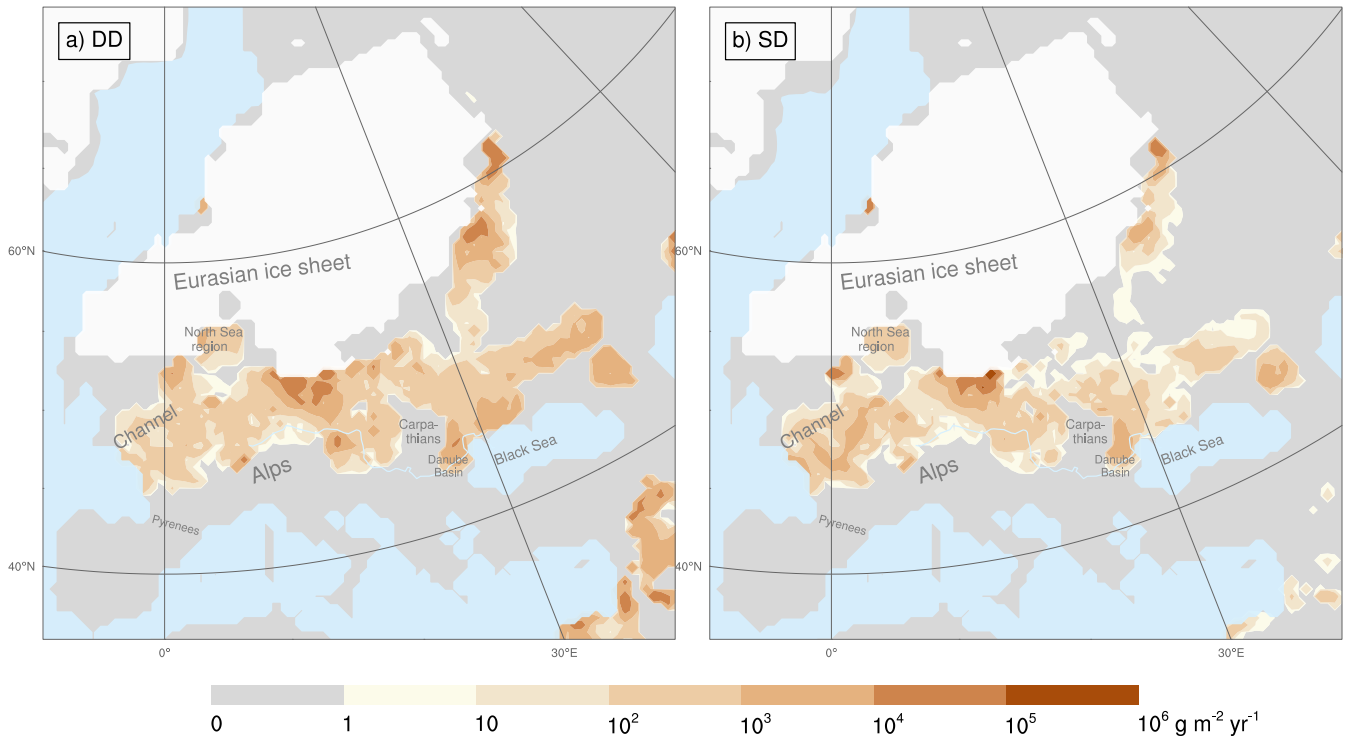


**Figure 3.** Dust emission rates for the Last Glacial Maximum. These reconstructions are based on a) dynamic downscaling (DD) and b) statistic dynamic downscaling (SD). Ice sheet extents (white overlay), Danube (light-blue line).

210 to calculate the spatial erodibility distribution. Based on this distribution, the WRF-Chem-LGM was able to suppress unrealistic  
 212 numerical dust emission from areas with low or zero erodibility. Most likely, the improvement results also from selecting the  
well-tested and observation-confirmed Shao dust emission scheme (Shao, 2004; Kang et al., 2011). For example, this scheme  
 214 takes into account the dynamic moisture changes at the soil surface. Due to our recent improvement of the Shao dust emission  
scheme, the effect of snow cover on dust emission has also been taken into account in the WRF-Chem-LGM experiments.

216 The MARs and MAR10 (Supplementary Table S1 and Fig. 4) are in better quantitative agreement (by orders of magnitude)  
with the loess-based reconstructed MARs were reconstructed from samples that were extracted during fieldwork campaigns  
from loess paleosol sites. The MAR for a specific site was inferred by taking into account all particles found in respective  
 218 sample, independent of their diameter. In contrast, the MAR10 for the same site was inferred by taking into account only  
particles up to 10  $\mu\text{m}$  diameter. Most of the MARs and MAR10 (Supplementary Table S1) and Fig. 4) result from sites of the  
 220 European loess belt. This belt plays a key role in assessing paleoclimatic dust cycle simulations for Europe  
(Kukla, 1977; Little et al., 2002; Haase et al., 2007; Sima et al., 2009). During the LGM, it corresponded approximately to the  
 222 fraction of the European land area that was bounded northwards by the EIS and southwards by the Alps, Dinaric Alps and Black  
Sea. For this study, the deposition rate of The  $F_{D20}$  in Figure 4a and b ( $F_{D12}$  in Fig. 4c and d) denote the WRF-Chem-LGM  
 224 deposition rates caused only by particles smaller than 12  $\mu\text{m}$  (20  $\mu\text{m}$  20  $\mu\text{m}$  (12  $\mu\text{m}$ ) in diameteris denoted as  $F_{DT2}$  ( $F_{D20}$ ).

~~$F_{D20}$  and  $F_{D12}$  are calculated based on the dynamic ( $F_{D20DD}$ ,  $F_{D12DD}$ ) and relate to the dynamic, while the  $F_{D20SD}$  and  $F_{D12SD}$  relate to the~~  
226 ~~downscaling methods, the  $F_{D20DD}$  and  $F_{D12DD}$  ) and relate to the dynamic, while the  $F_{D20SD}$  and  $F_{D12SD}$  relate to the~~  
statistic dynamic ( $F_{D20SD}$ ,  $F_{D12SD}$ ) downscaling simulations. ~~The dynamic and~~ For central Europe, the dynamic (Fig. 4a and  
228 ~~c) and~~ statistic dynamic downscaling (Fig. 4b and d) resulted in similar  $F_D$  values for central Europe, confirming the suitability  
of the statistic dynamic downscaling.

230 During the LGM, the largest  $F_{D20}$  ( $>10^5$  g m<sup>-2</sup> yr<sup>-1</sup>) occurred in western Poland (Fig. 4a). Slightly lower  $F_{D20}$  ( $10^4$ –  
 $10^5$  g m<sup>-2</sup> yr<sup>-1</sup>) were found in adjacent areas, e.g. in eastern Germany.  $F_{D20}$  was  $10^3$ – $10^4$  g m<sup>-2</sup> yr<sup>-1</sup> on the North German  
232 Plain, in the dry-fallen German Bight, eastern England, northern and western France, the Benelux and southeast of the Carpathi-  
ans. Regional deposition maxima of  $10^3$ – $10^4$  g m<sup>-2</sup> yr<sup>-1</sup> occurred along the French LGM coastline (46–48°N), on the eastern  
234 side of the Carpathians (44–47°N, including the eastern Romanian Danube Plain) and near the Caucasus (44–45°N, Fig. 4a).  
They coincide with today's extensive loess derivatives along the Atlantic coastline of France, at the European foothills north of  
236 42°N and with the loess thickness maximum in the Romanian Danube Plain (Haase et al., 2007; Jipa, 2014). The quality of the  
~~simulation is~~ ~~simulations is also~~ recognizable in the Carpathian Basin ~~where, which is now half covered with loess and clay of~~  
238 ~~aeolian origin (Varga et al., 2012). There,~~ the simulated  $F_{D20}$  of 100–1000 g m<sup>-2</sup> yr<sup>-1</sup> (Fig. 4a) are in good agreement with the  
MARs (200–500 g m<sup>-2</sup> yr<sup>-1</sup>) ~~and the fact that half of the Basin is covered by loess and clay of aeolian origin (Varga et al., 2012)~~  
240 ~~. By definition, the MAR is reconstructed from all deposited particles independent of their size.~~ In Ukraine and at the eastern  
margins of the EIS,  $F_{D20}$  of 100–1000 g m<sup>-2</sup> yr<sup>-1</sup> are in line with the MARs (Fig. 4a). Over Ukraine and consistent with our  
242 results, dust transport and deposition by east sector winds is evidenced by loess deposits on the west bank of the Dnieper (Sima  
et al., 2013).

244 The MARs of a few loess sites are higher than the  $F_{D20}$  in their surrounding. Such an underestimation could be explained  
by particles larger than 20 μm which are not taken into account by the  $F_{D20}$ . For some regions, the MARs of closely related  
246 sites vary over orders of magnitude, e.g. between  $10^2$  and  $10^4$  g m<sup>-2</sup> yr<sup>-1</sup> near the Rhine and in Belgium (Fig. 4a). This may  
be due to strong small scale variability, loess dating uncertainties (Singhvi et al., 2001; Renssen et al., 2007) or age model  
248 inaccuracies (Bettis et al., 2003). For western Germany, a transition from higher  $F_{D20}$  ( $10^3$ – $10^4$  g m<sup>-2</sup> yr<sup>-1</sup>) in its northeast  
to lower  $F_{D20}$  ( $10^2$ – $10^3$  g m<sup>-2</sup> yr<sup>-1</sup>) in its southwest was found (Fig. 4a). For a few sites in southwestern Germany, Austria,  
250 Ukraine and along the Danube,  $F_{D20}$  is an order of magnitude lower than the respective MARs (Fig. 4a). Given the 50 km grid  
spacing of the WRF-Chem-LGM simulation, this may be attributed to missing local dust sources, such as dry-fallen riverbeds  
252 and floodplains. Possibly, the MARs of these sites are also inferred from particles that were predominantly larger than 20 μm  
yet data on particle sizes is not available. ~~The peak deposition locations and the overall shape of the  $F_{D20}$  and  $F_{D12}$  patterns~~  
254 ~~are very similar (Fig. 4). The  $F_{D12}$  are also almost everywhere consistent with the MAR10 (Fig. 4c and d). Those  $F_{D12}$  that~~  
~~overestimate the MAR10 do not contradict the consistency since the  $F_{D12}$  also take into account particles that are (by definition)~~  
256 ~~excluded by the MAR10. In summary, large consistency was found between the simulated dust deposition rates and the MARs~~  
~~and MAR10 that were reconstructed from on-site samples.~~

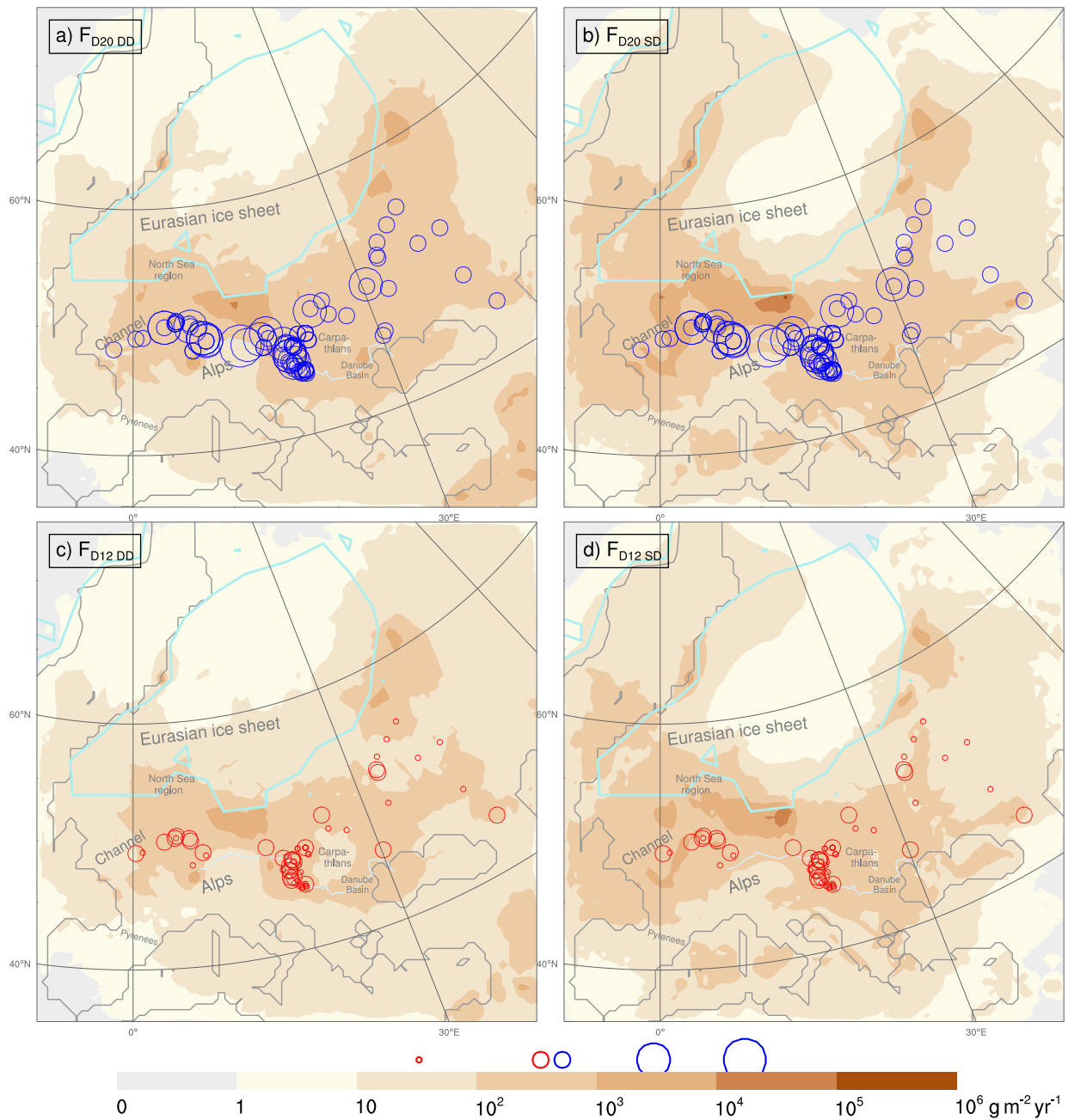


**Figure 4.** Dust deposition rates for the Last Glacial Maximum, comprising particles of up to 20  $\mu\text{m}$  diameter ( $F_{D20}$ ) using (a) dynamic downscaling ( $F_{D20\text{DD}}$ ) and (b) statistic dynamic downscaling ( $F_{D20\text{SD}}$ ). (c) and (d) as (a) and (b), but for particles up to 12  $\mu\text{m}$  ( $F_{D12}$ ). Each blue circle size represents one mass accumulation rate (MAR, [Supplementary Table S1 column 5](#)) magnitude. Each red circle size represents one reduced mass accumulation rate (MAR10, [Supplementary Table S1 column 6](#)) magnitude. MAR and MAR10 values compiled in Supplementary Table S1. The simulation-based ( $F_{D20}$ ,  $F_{D12}$ ) and the fieldwork-based (MAR, MAR10) rates result from independent data. Delineated are the Danube (light blue), the coastlines (grey; Braconnot et al., 2012) and the ice sheet extents (turquoise; Cline et al., 1984).

During the LGM, the strongest emission and deposition in Europe occurred in summer, followed by autumn and spring (Fig. 5 and 6). The areas with the overall highest emission were also those with the highest seasonal emission (Fig. 3 and 5). The spring and winter emissions have the same order of magnitude. The low winter and spring emission rates along the EIS margin were caused by the then extensive snow cover there. During winter, emissions peaked only in northern France, consistent with its small snow cover and the vegetation cover (Fig. 7) that was prescribed to the WRF-Chem-LGM. Major dust emissions occurred from the Carpathian Basin and along the northwest coast of the Black Sea. During spring, slightly attenuated emissions are simulated for France, despite of the decreasing snow cover but in accordance with its increasing vegetation cover. Considerably higher emission rates are simulated from along the German and Polish EIS margin where the snow cover had retreated. For eastern Europe, the growing vegetation cover and the slight soil moisture increase account for partly lower spring than winter emission rates. The soil moisture increase possibly resulted from meltwater of the retreating snow cover. The highest emission rates occurred during summer and were located along the German and Polish EIS margin. Slightly lower emissions are found to the east of the EIS. These findings are coherent with the surface properties of these areas during summer, i.e. they were mostly snow-free and the least moist. During fall, the snow cover increased, causing a decrease of dust emissions, except for the area north of the Black Sea which encountered its annual maximum. This maximum can be attributed to the retreat of the vegetation cover and the dry soil conditions there.

The winter CWT distribution indicates prevailing east sector winds (37%) in contrast to cyclonic regimes, which occurred much less frequently than on annual average (13%; Table 2 and 3). The winter deposition rates northwest of the Alps were considerably above, while the rates at the central and eastern European EIS margin were below the annual average (Fig. 4 and 6a). In western Europe, the highest deposition rates occurred near the sources, yet a considerable dust fraction was also transported and deposited to the west and northwest of the sources, which requires east sector winds. Low deposition rates were found for southern France, however marked depositions occurred when subjected to cyclonic regimes (Fig. 9b). The deposition pattern for the central Mediterranean area (Italy, the Adriatic) suggests significant dust transport by east sector winds and anticyclonic winds, in sum prevailing 51% of the times. In eastern Europe, considerable winter depositions rates covered areas south of the dust sources, in particular the western Black Sea and regions south of the Danube. This indicates a significant contribution to the dust transport by northerlies (6%), northeasters (12%) and the anticyclonic regimes (14%).

Also the spring deposition rates evidence the importance of the east sector winds (42%, Table 3) for the dust cycle. In western Europe, major deposition areas are to the west and northwest of the sources, while they are to the west and southwest in eastern Europe (Fig. 6b). An increase of the dust transport towards the south in western, and towards the north in eastern Europe indicates an increasing role of the cyclonic regimes (27%) during the spring.

The summer deposition rates are distributed zonally along the EIS margin, suggesting an approximately latitude-parallel dust transport by west (21%) and/or east sector (24%) wind directions. In addition, the northern flanks of cyclonic regimes (24%) likely contributed to a westwards dust transport. Over north-easternmost Europe (40E, 62N), the deposition rates suggest east sector winds. The autumn deposition rates over western and central Europe show a westward running plume from the southern

292 EIS margin over Germany and Poland, corroborating the major role of the east sector winds (38%) for the dust cycle. The high deposition rates in eastern Europe suggest that also the cyclonic regimes (19%) contributed during fall.

**Table 3.** Seasonal CWT occurrence frequencies (%) for central Europe (centered at 17.5°E and 47.5°N) during the LGM. The frequencies are based on MPI-LGM simulation. The CWT classes are: Cyclonic (C), Anticyclonic (A), Northeast (NE), East (E) followed by the remaining standard wind directions. Sum E is the sum of the east sector winds (NE, E, SE). The seasons are labeled DJF (winter), MAM (spring), JJA (summer) and SON (fall).

	C	A	Sum E	NE	E	SE	S	SW	W	NW	N
DJF	12.6	13.9	37.4	11.8	14.4	11.2	12.9	8.5	5.1	4.1	5.6
MAM	27.1	6.1	41.9	12.9	16.4	12.6	9.7	4.8	2.8	3.6	4.2
JJA	26.8	7.5	24.4	12.8	6.3	5.3	9.3	7.3	6.1	7.9	10.7
SON	18.6	10.0	37.8	12.8	13.6	11.4	10.8	6.8	3.8	5.1	7.0

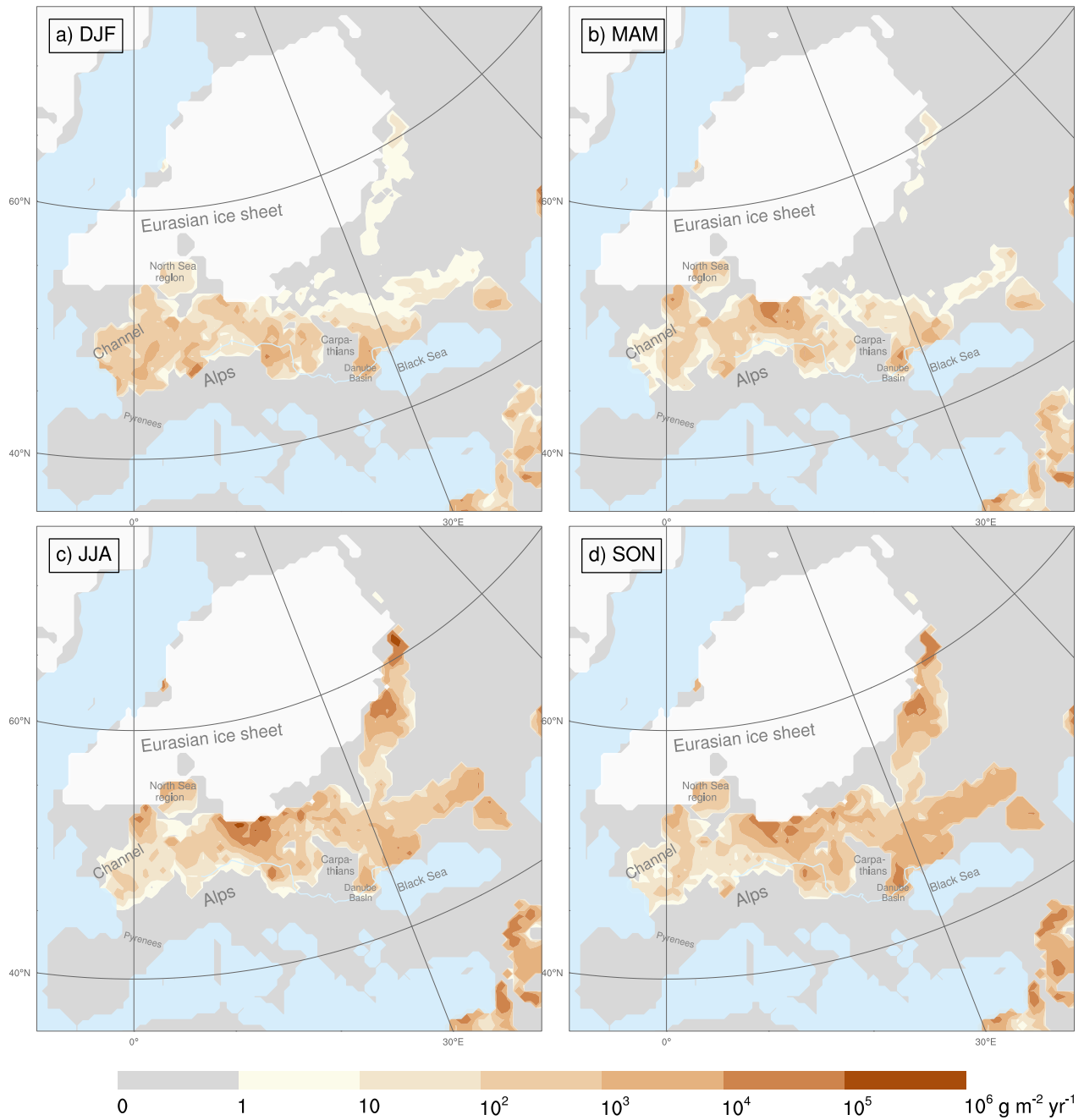


**Figure 5.** Dust emission rates for a) winter (DJF), b) spring (MAM), c) summer (JJA), and d) fall (SON) during the Last Glacial Maximum. This reconstruction is based on dynamic downscaling. The Danube (light-blue line) and the extent of the continental ice sheets (white) are shown.

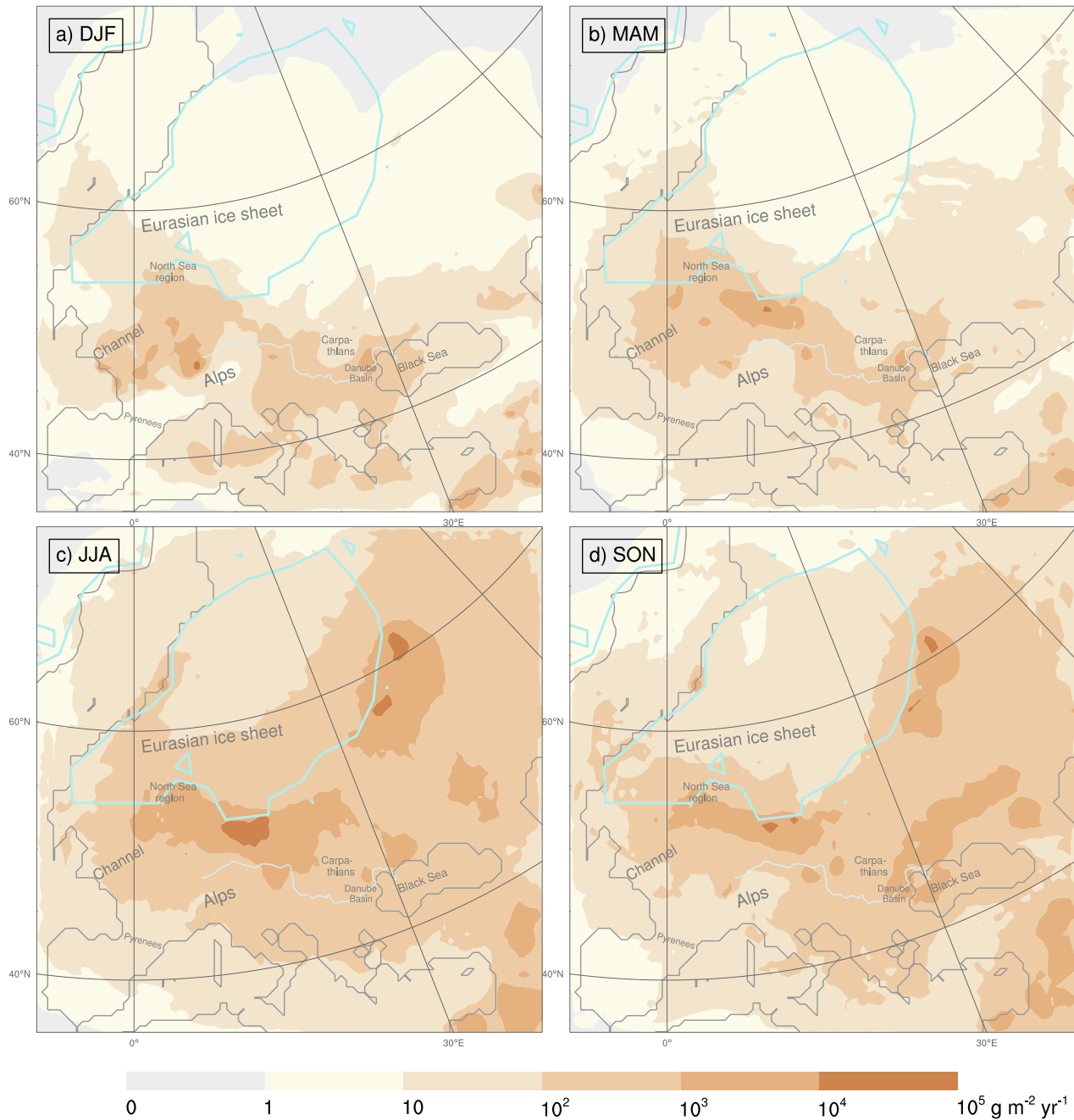


**Figure 6.** Dust deposition rates for a) winter (DJF), b) spring (MAM), c) summer (JJA) and d) autumn (SON) during the Last Glacial Maximum. This reconstruction is based on dynamic downscaling. Ice sheet extents (turquoise; Cline et al., 1984), Danube (light-blue line) and coastlines (grey; Braconnot et al., 2012) are delineated.

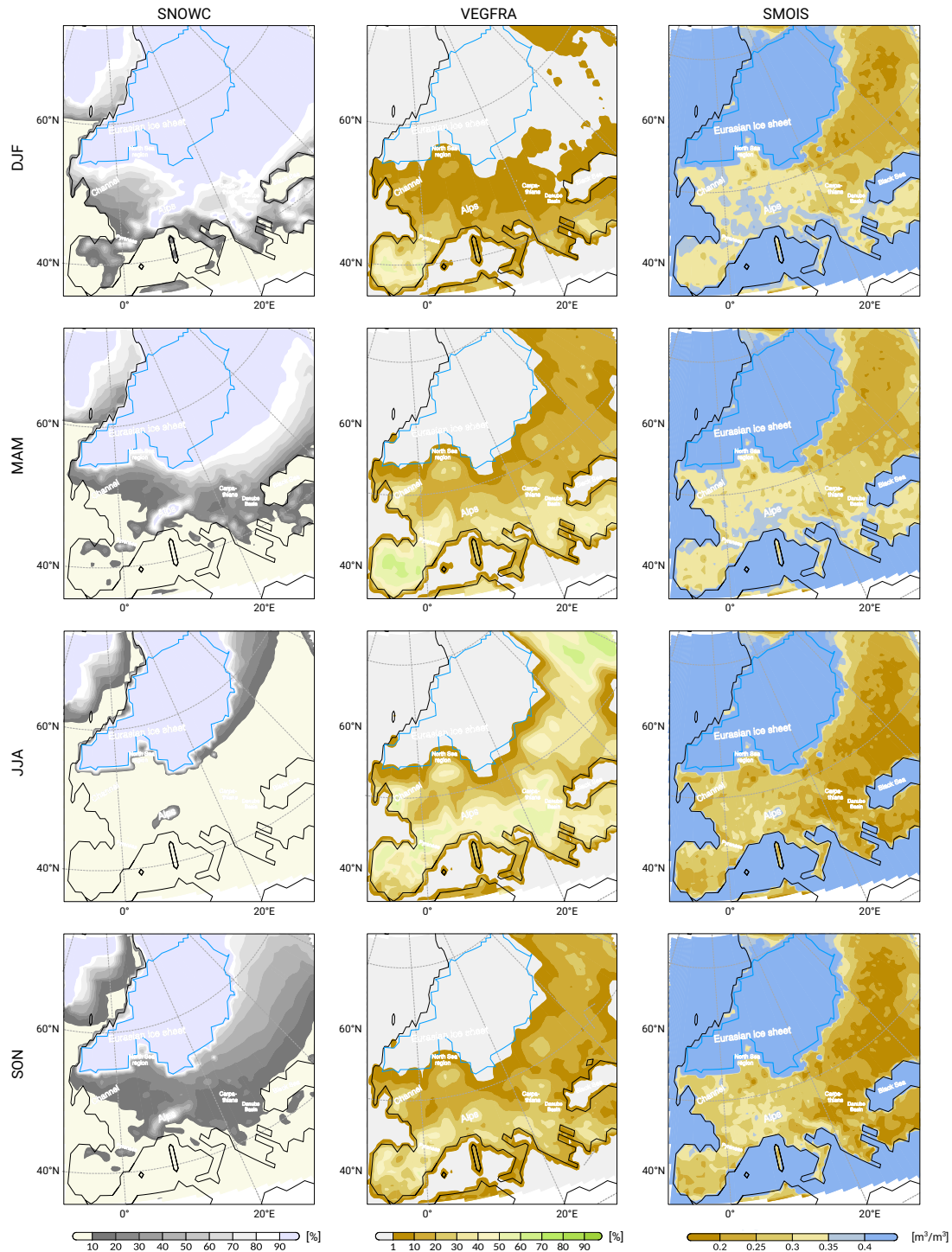


**Figure 7.** Snow cover (%), vegetation cover (%) and soil moisture ( $m^3/m^3$ ), resolved for winter (DJF), spring (MAM), summer (JJA) and fall (SON) for the Last Glacial Maximum. These reconstructions are based on dynamic downscaling.

### 294 3.6 Wind regime-based dust cycle decomposition

The wind regime occurrence frequency distribution (Table 2) demonstrates the temporal dominance of the east sector winds during the LGM. This temporal dominance likely shaped the dust cycle but the contribution of each wind regime type has so far not been analyzed. This analysis is provided here by discussing the dust emission and deposition characteristics associated with different CWTs which reveal that the east sector winds caused by far the largest dust emission and depositions during the LGM (Fig. 8a and 9a). In sum, they generated an average dust emission of  $1111 \text{ g m}^{-2} \text{ yr}^{-1}$  (Fig. 8a) which is more than twice of the rate generated by cyclonic regimes ( $494 \text{ g m}^{-2} \text{ yr}^{-1}$ , Fig. 8b). The west sector winds contributed on average even less to the dust cycle  $375 \text{ g m}^{-2} \text{ yr}^{-1}$  (Fig. 8c). Compared to the southerlies ( $232 \text{ g m}^{-2} \text{ yr}^{-1}$ , Fig. 8d), this rate is low for a wind sector that sums the contribution of three wind directions (SW, W, NW).

The cyclonic wind regimes caused the most heterogeneously distributed emissions (Fig. 8b) with four main centers: the largest located in the German-Polish-Czech border region, another in eastern England and the remaining two near the EIS margin in western Russia. This distribution resembles to a subset of the emission distribution of the east sector winds (Fig. 8a). Together with the location of the CWT reference regions, this resemblance could be explained by the fact that all records classified as cyclonic must center their cyclonic pressure distribution approximately around the central point for the CWT classification ( $17.5^\circ\text{E}$ ,  $47.5^\circ\text{N}$ ). This implies that the corresponding emissions could have been triggered by easterlies on the northern flanks of the cyclones. Dust was hardly emitted from areas on the southern flanks of the cyclones which are commonly affected by fronts and precipitation (Booth et al., 2018). In addition to the dust emission areas that occurred equally during both regimes (cyclonic and east sector winds), the east sector winds also generated emissions in Austria, Slovakia, Hungary, Ukraine, central Germany, the Danube Basin and the North Sea Basin. In contrast, the west sector winds produced a more homogeneous distribution of markedly smaller emission rates extending from western Ukraine to the French Atlantic coast. While northwesterly winds with a strong northerly component most likely forced emissions from the German-Polish EIS margin, the west sector winds and the southerlies controlled the emissions from France, southwestern Germany, the Channel, and the Alps foreland (Fig. 8c and d). The combination of the emission and deposition rate patterns of the east sector winds (Fig. 8a and 9a) indicates major westwards dust transport along the southern and eastern EIS margin. The conic shape of the deposition rate distribution in western and central Europe (between  $10^2$  and  $10^3 \text{ g m}^{-2} \text{ yr}^{-1}$ ) suggests that these depositions can be attributed to emissions from more eastern sources. The east sector winds also deposited considerable amounts of dust in and south of the Danube Basin as well as along the Danube.

The deposition rates of the cyclonic regimes (Fig. 9b) indicate two main dust transport directions: westwards over central and eastern Europe, whereas southwards over western Europe. More precisely, dust was transported westwards from Poland to eastern and central Germany, while it was carried southwards from eastern England to the Channel and north-western France up to the Pyrenees foreland. The emission and deposition distributions associated with the west sector winds are almost congruent (Fig. 8c and 9c). Combining them does not reveal a unique dust transport direction by west sector winds, it rather suggests omnidirectional transports; even a westward transport cannot be excluded e.g. to Scotland, Ireland or areas at the Russian EIS margin (Fig. 9c). The depositions caused by southerlies show a north-westward transport over central Europe (Fig. 9d).

328 Considerable amounts of dust (between  $10^3$  and  $10^5$  g m<sup>-2</sup> yr<sup>-1</sup>) were transported from sources in western Poland, eastern  
Germany and Czechia to northern Germany, Denmark, southern Sweden and the North Sea Basin. The deposition pattern also  
330 suggests a north-westward transport in France.

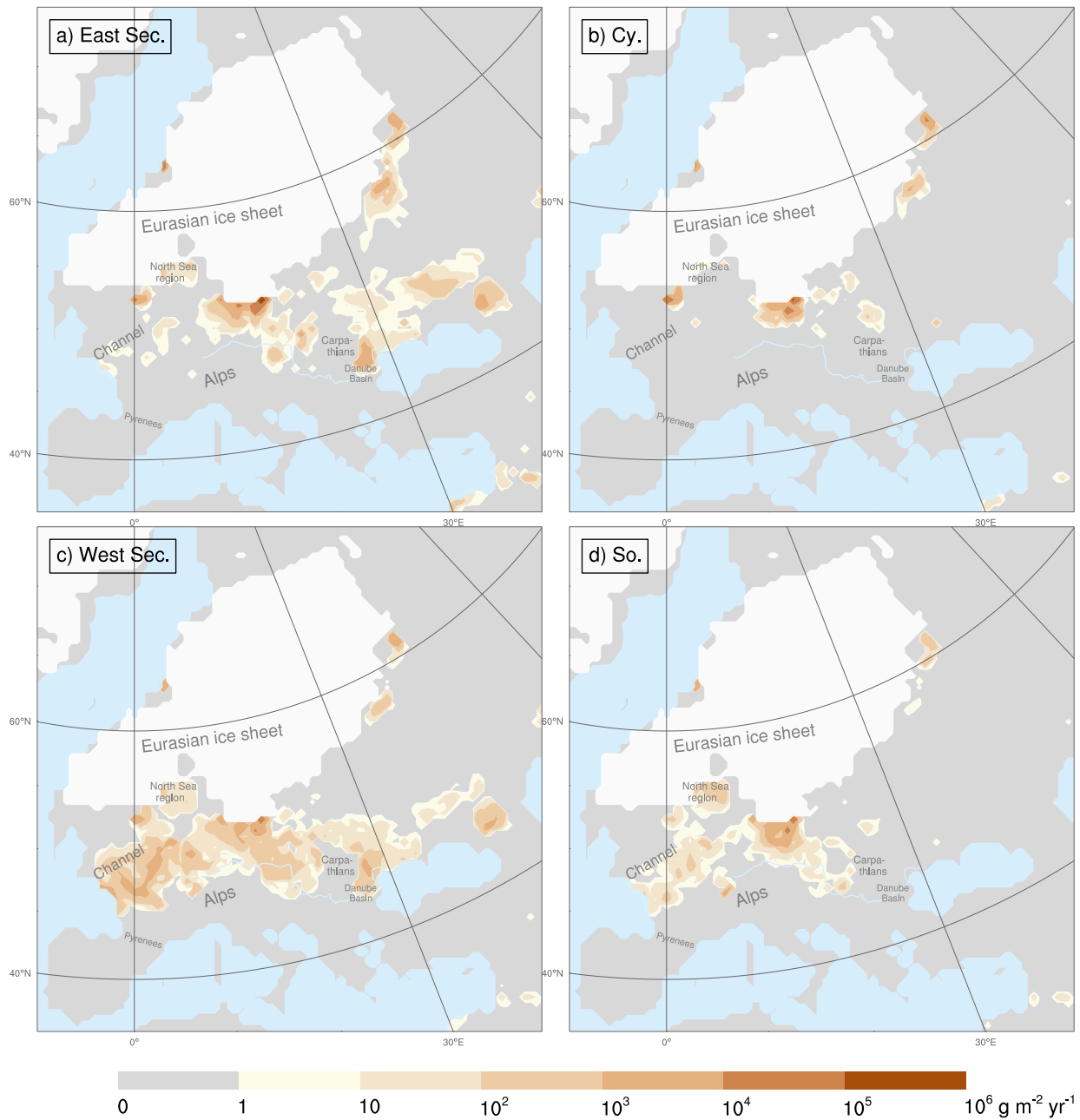


**Figure 8.** Dust emission rate fractions caused by the a) northeasters, easterlies and southeasters, b) cyclonic regimes, c) southwester, westerlies and northwester, and d) southerlies during the Last Glacial Maximum. The simulated emission rates are weighted according to the occurrence frequency of the associated wind regime(s) in the Max-Planck-Institute Earth System Model (Table 2). Dust particles up to 20  $\mu\text{m}$  diameter have been considered. The Danube (light-blue line) and the extent of the continental ice sheets (white) are shown.

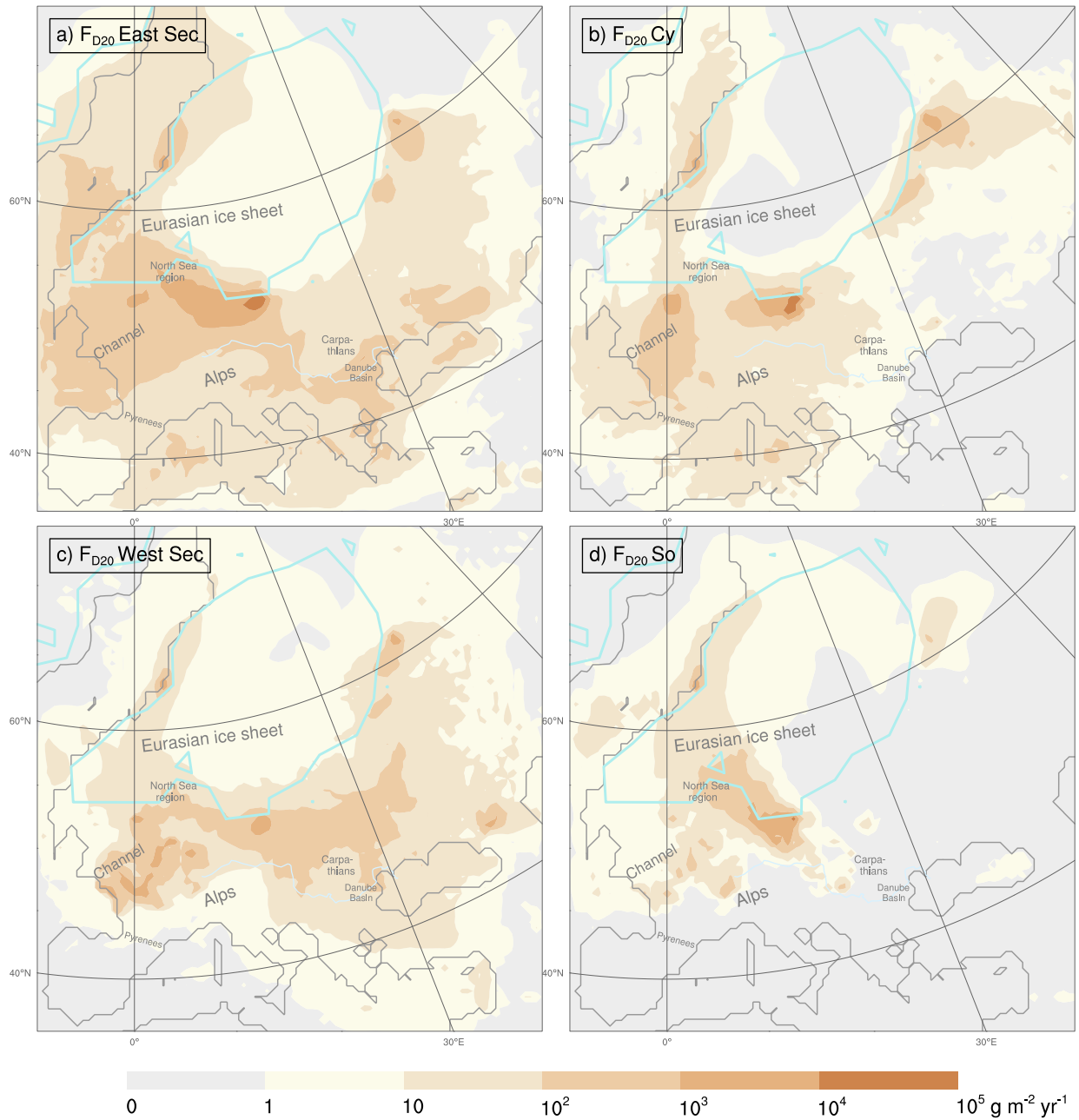


**Figure 9.** Dust deposition rate fractions caused solely by the a) northeasters, easterlies and southeasters, b) cyclonic regimes, c) southwesters, westerlies and northwesterlies, and d) the southerlies during the Last Glacial Maximum. The simulated deposition rates are weighted according to the occurrence frequency of the associated wind regime(s) in the Max-Planck-Institute Earth System Model (Table 2). Dust particles up to  $20 \mu\text{m}$  diameter have been considered. The ice sheet extents (turquoise; Cline et al., 1984), the Danube (light blue) and the coastlines (grey; Braconnot et al., 2012) are delineated.

## 4 Conclusions

332 Compared to previous climate-dust model simulations for the LGM, this study presents a dust cycle reconstruction with dust  
deposition rates that are in much better agreement with the MARs reconstructed from more than 70 different loess deposits  
334 across Europe. By taking into account the effect of different wind directions, a more complete understanding of the dust cycle  
is established. The obtained results corroborate the hypothesis on the linkage between the prevailing dry east sector winds as a  
336 major driver of the LGM dust cycle in central and eastern Europe and the loess deposits.

The study demonstrates that the WRF-Chem-LGM model is capable of simulating the glacial dust cycle including emission,  
338 transport and deposition. In addition, the suitability of the statistic dynamic approach for regional climate-dust simulations is  
proven by the similarity of the dynamic and statistic-dynamic downscaling results. In contrast to the dominant present-day  
340 westerlies over Europe, the CWT analysis revealed dominant east sector (36%) and cyclonic (22%) wind regimes during the  
LGM over central Europe. These east sector winds dominated the LGM dust cycle by far during all but the summer season.  
342 In summer, they were about as frequent as the cyclonic regimes. The dominance of the east sector winds during the LGM is  
corroborated by numerous local proxies for the wind and dust transport directions in Europe.

344 The WRF-Chem-LGM simulations show that almost all dust emission occurred in a corridor that was bounded to the north  
by the EIS and to the south by the Alps and the Black Sea. Within this corridor, the highest emissions were generated from the  
346 dry-fallen flats, the lowlands bordering mountain slopes, and the proglacial areas of the EIS. Most dust was emitted during the  
summers and autumns of the LGM, probably due to the then vanishing snow cover. The largest ~~depositions~~ dust deposition rates  
348 during the LGM occurred near the southernmost margin of the EIS (12–19°E;  $10^5 \text{ g m}^{-2} \text{ yr}^{-1}$ ), on the North German Plain in-  
cluding adjacent regions and in the southern North Sea region. The agreement between the performed climate-dust simulations  
350 for the LGM and the reconstructed MARs from loess deposits corroborates the proposed LGM dust cycle hypothesis.

*Author contributions.* EJS, PL and YS designed the concept of the study. PL performed the dynamic downscaling simulation and created  
352 Figure 7. EJS performed the statistic dynamic downscaling, compared the results with the proxy data including the reconstructed loess mass  
accumulation rates, created the tables and the remaining figures. EJS wrote the paper with contributions from PL and YS.

354 *Competing interests.* The authors declare that they have no conflict of interest.

*Acknowledgements.* This research was funded by the Deutsche Forschungsgemeinschaft (DFG) through the Collaborative Research Center  
356 806 “Our Way to Europe” (CRC806). P. Ludwig thanks the Helmholtz initiative REKLIM for funding. We thank the German Climate  
Computing Centre (DKRZ, Hamburg) for providing the MPI-ESM data and computing resources (project 965). We thank the Regional  
358 Computing Center (University of Cologne) for providing support and computing time on the high performance computing system CHEOPS.

We thank Qian Xia for preparing model boundary condition data. We thank F. Lehmkuhl, the CRC806 (second phase) members of his group  
360 and J. G. Pinto for helpful discussions and comments.

## References

- 362 Albani, S., Mahowald, N. M., Murphy, L. N., Raiswell, R., Moore, J. K., Anderson, R. F., McGee, D., Bradtmiller, L. I., Delmonte, B.,  
Hesse, P. P., and Mayewski, P. A.: Paleodust variability since the Last Glacial Maximum and implications for iron inputs to the ocean,  
364 *Geophysical Research Letters*, 43, 3944–3954, <https://doi.org/10.1002/2016GL067911>, 2016.
- Antoine, P., Rousseau, D.-D., Fuchs, M., Hatté, C., Gauthier, C., Marković, S. B., Jovanović, M., Gaudenyi, T., Moine, O., and Rossignol, J.:  
366 High-resolution record of the last climatic cycle in the southern Carpathian Basin (Surduk, Vojvodina, Serbia), *Quaternary International*,  
198, 19–36, <http://dx.doi.org/10.1016/j.quaint.2008.12.008>, 2009a.
- 368 Antoine, P., Rousseau, D.-D., Moine, O., Kunesch, S., Hatté, C., Lang, A., Tissoux, H., and Zöller, L.: Rapid and cyclic aeolian deposition  
during the Last Glacial in European loess: a high-resolution record from Nussloch, Germany, *Quaternary Science Reviews*, 28, 2955–2973,  
370 <http://dx.doi.org/10.1016/j.quascirev.2009.08.001>, 2009b.
- Austermann, J., Mitrovica, J. X., Latychev, K., and Milne, G. A.: Barbados-based estimate of ice volume at Last Glacial Maximum affected  
372 by subducted plate, *Nature Geoscience*, 6, 553–557, <https://doi.org/10.1038/ngeo1859>, 2013.
- Bartlein, P. J., Harrison, S. P., Brewer, S., Connor, S., Davis, B. A. S., Gajewski, K., Guiot, J., Harrison-Prentice, T. I., Henderson, A.,  
374 Peyron, O., and et al.: Pollen-based continental climate reconstructions at 6 and 21 ka: a global synthesis, *Climate Dynamics*, 37, 775–802,  
<http://dx.doi.org/10.1007/s00382-010-0904-1>, 2011.
- 376 Baumann-Stanzer, K., Greilinger, M., Kasper-Giebl, A., Flandorfer, C., Hieden, A., Lotteraner, C., Ortner, M., Vergeiner, J., Schauer, G., and  
Piringer, M.: Evaluation of WRF-Chem Model Forecasts of a Prolonged Saharan Dust Episode over the Eastern Alps, *Aerosol and Air*  
378 *Quality Research*, 19, 1226–1240, 2019.
- Bettis, E. A., Muhs, D. R., Roberts, H. M., and Wintle, A. G.: Last Glacial loess in the conterminous USA, *Quaternary Science Reviews*, 22,  
380 1907–1946, [http://dx.doi.org/10.1016/S0277-3791\(03\)00169-0](http://dx.doi.org/10.1016/S0277-3791(03)00169-0), 2003.
- Bian, H., Tie, X., Cao, J., Ying, Z., Han, S., Xue, Y., et al.: Analysis of a severe dust storm event over China: application of the WRF-dust  
382 model, *Aerosol and Air Quality Research*, 11, 419–428, 2011.
- Bokhorst, M., Vandenberghe, J., Sümegei, P., Łanczont, M., Gerasimenko, N., Matviishina, Z., Marković, S., and Frechen, M.: Atmospheric  
384 circulation patterns in central and eastern Europe during the Weichselian Pleniglacial inferred from loess grain-size records, *Quaternary*  
*International*, 234, 62–74, <http://dx.doi.org/10.1016/j.quaint.2010.07.018>, 2011.
- 386 Booth, J. F., Naud, C. M., and Willison, J.: Evaluation of Extratropical Cyclone Precipitation in the North Atlantic Basin: An Analysis of  
ERA-Interim, WRF, and Two CMIP5 Models, *J. of Climate*, 31, 2345–2360, <https://doi.org/10.1175/JCLI-D-17-0308.1>, <https://doi.org/10.1175/JCLI-D-17-0308.1>, 2018.
- 388 Braconnot, P., Harrison, S. P., Kageyama, M., Bartlein, P. J., Masson-Delmotte, V., Abe-Ouchi, A., Otto-Bliesner, B., and Zhao, Y.: Evaluation  
of climate models using palaeoclimatic data, *Nature Climate Change*, 2, 417–424, <http://dx.doi.org/10.1038/nclimate1456>, 2012.
- 390 Buggle, B., Glaser, B., Zöller, L., Hambach, U., Marković, S., Glaser, I., and Gerasimenko, N.: Geochemical characterization and origin of  
392 Southeastern and Eastern European loesses (Serbia, Romania, Ukraine), *Quaternary Science Reviews*, 27, 1058–1075, <http://dx.doi.org/10.1016/j.quascirev.2008.01.018>, 2008.
- 394 Chin, M., Rood, R. B., Lin, S.-J., Müller, J.-F., and Thompson, A. M.: Atmospheric sulfur cycle simulated in the global model GO-  
CART: Model description and global properties, *J. of Geophysical Research: Atmospheres*, 105, 24 671–24 687, <http://dx.doi.org/10.1029/2000JD900384>, 2000.
- 396

Chin, M., Ginoux, P., Kinne, S., Torres, O., Holben, B. N., Duncan, B. N., Martin, R. V., Logan, J. A., Higurashi, A., and Nakajima, T.:  
398 Tropospheric Aerosol Optical Thickness from the GOCART Model and Comparisons with Satellite and Sun Photometer Measurements, *J.*  
of the Atmospheric Sciences, 59, 461–483, [https://doi.org/10.1175/1520-0469\(2002\)059<0461:taotft>2.0.co;2](https://doi.org/10.1175/1520-0469(2002)059<0461:taotft>2.0.co;2), [http://dx.doi.org/10.1175/](http://dx.doi.org/10.1175/1520-0469(2002)059<0461:TAOTFT>2.0.CO;2)  
400 1520-0469(2002)059<0461:TAOTFT>2.0.CO;2, 2002.

Clark, P. U. and Mix, A. C.: Ice sheets and sea level of the Last Glacial Maximum, *Quaternary Science Reviews*, 21, 1–7,  
402 [https://doi.org/10.1016/S0277-3791\(01\)00118-4](https://doi.org/10.1016/S0277-3791(01)00118-4), 2002.

Clark, P. U., Dyke, A. S., Shakun, J. D., Carlson, A. E., Clark, J., Wohlfarth, B., Mitrovica, J. X., Hostetler, S. W., and McCabe, A. M.:  
404 The Last Glacial Maximum, *Science*, 325, 710–714, <https://doi.org/10.1126/science.1172873>, <http://dx.doi.org/10.1126/science.1172873>,  
2009.

406 Cline, R. M. L., Hays, J. D., Prell, W. L., Ruddiman, W. F., Moore, T. C., Kipp, N. G., Molino, B. E., Denton, G. H., Hughes, T. J., and  
Balsam, W. L.: The Last Interglacial Ocean, *Quaternary Research*, 21, 123–224, [https://doi.org/10.1016/0033-5894\(84\)90098-X](https://doi.org/10.1016/0033-5894(84)90098-X), 1984.

408 COHMAP Members: Climatic Changes of the Last 18,000 Years: Observations and Model Simulations, *Science*, 241, 1043–1052,  
<https://doi.org/10.1126/science.241.4869.1043>, 1988.

410 Darnenova, K., Sokolik, I. N., Shao, Y., Marticorena, B., and Bergametti, G.: Development of a physically based dust emission module  
within the Weather Research and Forecasting (WRF) model: Assessment of dust emission parameterizations and input parameters for  
412 source regions in Central and East Asia, *J. of Geophysical Research: Atmospheres*, 114, D14201, <https://doi.org/10.1029/2008JD011236>,  
2009.

414 Dietrich, S. and Seelos, K.: The reconstruction of easterly wind directions for the Eifel region (Central Europe) during the period 40.3 to  
12.9 ka BP, *Climate of the Past*, 6, 145–154, <http://dx.doi.org/10.5194/cp-6-145-2010>, 2010.

416 Fast, J. D., Gustafson, W. I., Easter, R. C., Zaveri, R. A., Barnard, J. C., Chapman, E. G., Grell, G. A., and Peckham, S. E.: Evolution of  
ozone, particulates, and aerosol direct radiative forcing in the vicinity of Houston using a fully coupled meteorology-chemistry-aerosol  
418 model, *J. of Geophysical Research: Atmospheres*, 111, n/a–n/a, <http://dx.doi.org/10.1029/2005JD006721>, d21305, 2006.

Fitzsimmons, K. E. and Hambach, U.: Loess accumulation during the last glacial maximum: Evidence from Urluia, southeastern Romania,  
420 *Quaternary International*, 334–335, 74–85, <https://doi.org/10.1016/j.quaint.2013.08.005>, <http://dx.doi.org/10.1016/j.quaint.2013.08.005>,  
2014.

422 Fitzsimmons, K. E., Marković, S. B., and Hambach, U.: Pleistocene environmental dynamics recorded in the loess of the middle and lower  
Danube basin, *Quaternary Science Reviews*, 41, 104–118, <http://dx.doi.org/10.1016/j.quascirev.2012.03.002>, 2012.

424 Florineth, D. and Schlüchter, C.: Alpine Evidence for Atmospheric Circulation Patterns in Europe during the Last Glacial Maximum, *Qua-*  
*ternary Research*, 54, 295–308, <http://dx.doi.org/10.1006/qres.2000.2169>, 2000.

426 Gasse, F., Vidal, L., Develle, A.-L., and Van Campo, E.: Hydrological variability in the Northern Levant: a 250 ka multiproxy record from  
the Yammoûneh (Lebanon) sedimentary sequence, *Climate of the Past*, 7, 1261–1284, <http://dx.doi.org/10.5194/cp-7-1261-2011>, 2011.

428 Ginoux, P., Chin, M., Tegen, I., Prospero, J. M., Holben, B., Dubovik, O., and Lin, S.-J.: Sources and distributions of dust aerosols simulated  
with the GOCART model, *J. of Geophysical Research: Atmospheres*, 106, 20 255–20 273, <http://dx.doi.org/10.1029/2000JD000053>, 2001.

430 Ginoux, P., Prospero, J. M., Torres, O., and Chin, M.: Long-term simulation of global dust distribution with the GOCART model: correlation  
with North Atlantic Oscillation, *Environmental Modelling & Software*, 19, 113–128, [https://doi.org/10.1016/s1364-8152\(03\)00114-2](https://doi.org/10.1016/s1364-8152(03)00114-2),  
432 [http://dx.doi.org/10.1016/S1364-8152\(03\)00114-2](http://dx.doi.org/10.1016/S1364-8152(03)00114-2), 2004.

- Giorgetta, M. A., Jungclaus, J., Reick, C. H., Legutke, S., Bader, J., Böttinger, M., Brovkin, V., Crueger, T., Esch, M., Fieg, K., and et al.:  
434 Climate and carbon cycle changes from 1850 to 2100 in MPI-ESM simulations for the Coupled Model Intercomparison Project phase 5,  
J. of Advances in Modeling Earth Systems, 5, 572–597, <http://dx.doi.org/10.1002/jame.20038>, 2013.
- 436 Grell, G. A., Peckham, S. E., Schmitz, R., McKeen, S. A., Frost, G., Skamarock, W. C., and Eder, B.: Fully coupled “online” chemistry  
within the WRF model, Atmospheric Environment, 39, 6957–6975, <http://dx.doi.org/10.1016/j.atmosenv.2005.04.027>, 2005.
- 438 Haase, D., Fink, J., Haase, G., Ruske, R., Pécsi, M., Richter, H., Altermann, M., and Jäger, K.-D.: Loess in Europe—its spatial distribution  
based on a European Loess Map, scale 1:2,500,000, Quaternary Science Reviews, 26, 1301–1312, [http://dx.doi.org/10.1016/j.quascirev.](http://dx.doi.org/10.1016/j.quascirev.2007.02.003)  
440 2007.02.003, 2007.
- Heyman, B. M., Heyman, J., Fickert, T., and Harbor, J. M.: Paleo-climate of the central European uplands during the last glacial maximum  
442 based on glacier mass-balance modeling, Quaternary Research, 79, 49–54, <http://dx.doi.org/10.1016/j.yqres.2012.09.005>, 2013.
- Hofer, D., Raible, C. C., Dehnert, A., and Kuhlemann, J.: The impact of different glacial boundary conditions on atmospheric dynamics and  
444 precipitation in the North Atlantic region, Climate of the Past, 8, 935–949, <http://dx.doi.org/10.5194/cp-8-935-2012>, 2012.
- Hopcroft, P. O., Valdes, P. J., Woodward, S., and Joshi, M. M.: Last glacial maximum radiative forcing from mineral dust aerosols in an Earth  
446 system model, J. of Geophysical Research: Atmospheres, 120, 8186–8205, <https://doi.org/10.1002/2015JD023742>, 2015.
- Hughes, A. L. C., Gyllencreutz, R., Lohne, O. S., Mangerud, J., and Svendsen, J. I.: The last Eurasian ice sheets - a chronological database  
448 and time-slice reconstruction, DATED-1, Boreas, 45, 1–45, <http://dx.doi.org/10.1111/bor.12142>, 2015.
- Jipa, D. C.: The conceptual sedimentary model of the Lower Danube loess basin: Sedimentogenetic implications, Quaternary International,  
450 351, 14–24, <http://dx.doi.org/10.1016/j.quaint.2013.06.008>, 2014.
- Jones, P. D., Hulme, M., and Briffa, K. R.: A comparison of Lamb circulation types with an objective classification scheme, International J.  
452 of Climatology, 13, 655–663, <https://doi.org/10.1002/joc.3370130606>, <http://dx.doi.org/10.1002/joc.3370130606>, 1993.
- Jones, P. D., Harpham, C., and Briffa, K. R.: Lamb weather types derived from reanalysis products, International J. of Climatology, 33,  
454 1129–1139, <https://doi.org/10.1002/joc.3498>, <http://dx.doi.org/10.1002/joc.3498>, 2013.
- Jung, E., Shao, Y., and Sakai, T.: A study on the effects of convective transport on regional-scale Asian dust storms in 2002, J. of Geophysical  
456 Research: Atmospheres, 110, <http://dx.doi.org/10.1029/2005JD005808>, d20201, 2005.
- Jungclaus, J., Giorgetta, M., Reick, C., Legutke, S., Brovkin, V., Crueger, T., Esch, M., Fieg, K., Fischer, N., Glushak, K., Gayler, V.,  
458 Haak, H., Hollweg, H.-D., Kinne, S., Kornblueh, L., Matei, D., Mauritsen, T., Mikolajewicz, U., Müller, W., Notz, D., Pohlmann,  
T., Raddatz, T., Rast, S., Roeckner, E., Salzmann, M., Schmidt, H., Schnur, R., Segschneider, J., Six, K., Stockhause, M., Weg-  
460 ner, J., Widmann, H., Wieners, K.-H., Claussen, M., Marotzke, J., and Stevens, B.: CMIP5 simulations of the Max Planck In-  
stitute for Meteorology (MPI-M) based on the MPI-ESM-P model: The Igm experiment, served by ESGF, WDCC at DKRZ,  
462 <https://doi.org/10.1594/WDCC/CMIP5.MXEPIg>, 2012.
- Jungclaus, J. H., Fischer, N., Haak, H., Lohmann, K., Marotzke, J., Matei, D., Mikolajewicz, U., Notz, D., and von Storch, J. S.: Character-  
464 istics of the ocean simulations in the Max Planck Institute Ocean Model (MPIOM) the ocean component of the MPI-Earth system model,  
J. of Advances in Modeling Earth Systems, 5, 422–446, <http://dx.doi.org/10.1002/jame.20023>, 2013.
- 466 Kang, J.-Y., Yoon, S.-C., Shao, Y., and Kim, S.-W.: Comparison of vertical dust flux by implementing three dust emission schemes in WR-  
F/Chem, J. of Geophysical Research: Atmospheres, 116, D09202, <https://doi.org/10.1029/2010JD014649>, [https://agupubs.onlinelibrary.](https://agupubs.onlinelibrary.wiley.com/doi/abs/10.1029/2010JD014649)  
468 [wiley.com/doi/abs/10.1029/2010JD014649](https://doi.org/10.1029/2010JD014649), 2011.
- Kaplan, J. O., Bigelow, N. H., Prentice, I. C., Harrison, S. P., Bartlein, P. J., Christensen, T. R., Cramer, W., Matveyeva, N. V., McGuire,  
470 A. D., Murray, D. F., Razzhivin, V. Y., Smith, B., Walker, D. A., Anderson, P. M., Andreev, A. A., Brubaker, L. B., Edwards, M. E.,

and Lozhkin, A. V.: Climate change and Arctic ecosystems: 2. Modeling, paleodata-model comparisons, and future projections, *J. of Geophysical Research: Atmospheres*, 108, <http://dx.doi.org/10.1029/2002JD002559>, 2003.

472 Krauß, L., Zens, J., Zeeden, C., Schulte, P., Eckmeier, E., and Lehmkuhl, F.: A Multi-Proxy Analysis of two Loess-Paleosol Sequences in  
474 the Northern Harz Foreland, Germany, *Palaeogeography, Palaeoclimatology, Palaeoecology*, 461, 401–417, <http://dx.doi.org/10.1016/j.palaeo.2016.09.001>, 2016.

476 Krinner, G., Mangerud, J., Jakobsson, M., Crucifix, M., Ritz, C., and Svendsen, J. I.: Enhanced ice sheet growth in Eurasia owing to adjacent  
ice-dammed lakes, *Nature*, 427, 429–432, <http://dx.doi.org/10.1038/nature02233>, 2004.

478 Kukla, G.: Pleistocene land—sea correlations I. Europe, *Earth-Science Reviews*, 13, 307–374, [http://dx.doi.org/10.1016/0012-8252\(77\)90125-8](http://dx.doi.org/10.1016/0012-8252(77)90125-8), 1977.

480 Kumar, R., Barth, M. C., Pfister, G. G., Naja, M., and Brasseur, G. P.: WRF-Chem simulations of a typical pre-monsoon dust storm  
in northern India: influences on aerosol optical properties and radiation budget, *Atmospheric Chemistry & Physics*, 14, 2431–2446,  
482 <https://doi.org/10.5194/acp-14-2431-2014>, 2014.

Lambeck, K., Rouby, H., Purcell, A., Sun, Y., and Sambridge, M.: Sea level and global ice volumes from the Last Glacial Maximum to the  
484 Holocene, *Proceedings of the National Academy of Science*, 111, 15 296–15 303, <https://doi.org/10.1073/pnas.1411762111>, 2014.

Laîné, A., Kageyama, M., Salas-Mélia, D., Voldoire, A., Rivière, G., Ramstein, G., Planton, S., Tyteca, S., and Peterschmitt, J. Y.: Northern  
486 hemisphere storm tracks during the last glacial maximum in the PMIP2 ocean-atmosphere coupled models: energetic study, seasonal  
cycle, precipitation, *Climate Dynamics*, 32, 593–614, <http://dx.doi.org/10.1007/s00382-008-0391-9>, 2009.

488 Little, E. C., Lian, O. B., Velichko, A., Morozova, T., Nechaev, V., Dlussky, K., and Rutter, N.: Quaternary stratigraphy and optical dating of  
loess from the east European Plain (Russia), *Quaternary Science Reviews*, 21, 1745–1762, [https://doi.org/10.1016/s0277-3791\(01\)00151-](https://doi.org/10.1016/s0277-3791(01)00151-2)  
490 2, 2002.

Ludwig, P., Schaffernicht, E. J., Shao, Y., and Pinto, J. G.: Regional atmospheric circulation over Europe during the Last Glacial Maximum  
492 and its links to precipitation, *J. of Geophysical Research: Atmospheres*, 121, 2130–2145, <http://dx.doi.org/10.1002/2015JD024444>, 2016.

Ludwig, P., Pinto, J. G., Raible, C. C., and Shao, Y.: Impacts of Surface Boundary Conditions on Regional Climate Model Simulations of  
494 European Climate during the Last Glacial Maximum, *Geophysical Research Letters*, <http://dx.doi.org/10.1002/2017GL073622>, 2017.

Ludwig, P., Gómez-Navarro, J. J., Pinto, J. G., Raible, C. C., Wagner, S., and Zorita, E.: Perspectives of regional paleoclimate modeling,  
496 *Ann. N.Y. Acad. Sci.*, 1436, 54–69, <https://doi.org/10.1111/nyas.13865>, <https://doi.org/10.1111/nyas.13865>, 2019.

Luetscher, M., Boch, R., Sodemann, H., Spötl, C., Cheng, H., Edwards, R. L., Frisia, S., Hof, F., and Müller, W.: North At-  
498 lantic storm track changes during the Last Glacial Maximum recorded by Alpine speleothems, *Nature Communications*, 6, 6344,  
<https://doi.org/10.1038/ncomms7344>, 2015.

500 Mahowald, N. M., Muhs, D. R., Levis, S., Rasch, P. J., Yoshioka, M., Zender, C. S., and Luo, C.: Change in atmospheric mineral aerosols  
in response to climate: Last glacial period, preindustrial, modern, and doubled carbon dioxide climates, *J. of Geophysical Research:*  
502 *Atmospheres*, 111, <http://dx.doi.org/10.1029/2005JD006653>, 2006.

Monnin, E., Indermühle, A., Dällenbach, A., Flückiger, J., Stauffer, B., Stocker, T. F., Raynaud, D., and Barnola, J.-M.: Atmospheric CO<sub>2</sub>  
504 Concentrations over the Last Glacial Termination, *Science*, 291, 112–114, <http://science.sciencemag.org/content/291/5501/112>, 2001.

Peyron, O., Guiot, J., Cheddadi, R., Tarasov, P., Reille, M., de Beaulieu, J.-L., Bottema, S., and Andrieu, V.: Climatic Reconstruction in  
506 Europe for 18,000 YR B.P. from Pollen Data, *Quaternary Research*, 49, 183–196, <http://dx.doi.org/10.1006/qres.1997.1961>, 1998.

Prentice, I. C. and Harrison, S. P.: Ecosystem effects of CO<sub>2</sub> concentration: evidence from past climates, *Climate of the Past*, 5, 297–307,  
508 <http://dx.doi.org/10.5194/cp-5-297-2009>, 2009.

Renssen, H., Kasse, C., Vandenberghe, J., and Lorenz, S. J.: Weichselian Late Pleniglacial surface winds over northwest and central Europe: a model–data comparison, *J. of Quaternary Science*, 22, 281–293, <http://dx.doi.org/10.1002/jqs.1038>, 2007.

Reyers, M., Pinto, J. G., and Moemken, J.: Statistical-dynamical downscaling for wind energy potentials: evaluation and applications to decadal hindcasts and climate change projections, *International J. of Climatology*, 35, 229–244, <https://doi.org/10.1002/joc.3975>, <http://dx.doi.org/10.1002/joc.3975>, 2014.

Rizza, U., Anabor, V., Mangia, C., Miglietta, M. M., Degrazia, G. A., and Passerini, G.: WRF-Chem simulation of a saharan dust outbreak over the mediterranean regions., *Ciência e Natura*, 38, 330–336, 2016.

Römer, W., Lehmkuhl, F., and Sirocko, F.: Late Pleistocene aeolian dust provenances and wind direction changes reconstructed by heavy mineral analysis of the sediments of the Dehner dry maar (Eifel, Germany), *Global and Planetary Change*, 147, 25–39, <http://dx.doi.org/10.1016/j.gloplacha.2016.10.012>, 2016.

Shao, Y.: Simplification of a dust emission scheme and comparison with data, *J. of Geophysical Research*, 109, <http://dx.doi.org/10.1029/2003JD004372>, 2004.

Shao, Y., Ishizuka, M., Mikami, M., and Leys, J. F.: Parameterization of size-resolved dust emission and validation with measurements, *J. of Geophysical Research: Atmospheres*, 116, D08 203, <https://doi.org/10.1029/2010JD014527>, <https://agupubs.onlinelibrary.wiley.com/doi/10.1029/2010JD014527>, 2011a.

Shao, Y., Wyrwoll, K.-H., Chappell, A., Huang, J., Lin, Z., McTainsh, G. H., Mikami, M., Tanaka, T. Y., Wang, X., and Yoon, S.: Dust cycle: An emerging core theme in Earth system science, *Aeolian Research*, 2, 181–204, <https://doi.org/10.1016/j.aeolia.2011.02.001>, <http://dx.doi.org/10.1016/j.aeolia.2011.02.001>, 2011b.

Shao, Y., Anhäuser, A., Ludwig, P., Schlüter, P., and Williams, E.: Statistical reconstruction of global vegetation for the last glacial maximum, *Global and Planetary Change*, 168, 67 – 77, <http://www.sciencedirect.com/science/article/pii/S0921818117306148>, 2018.

Sima, A., Rousseau, D.-D., Kageyama, M., Ramstein, G., Schulz, M., Balkanski, Y., Antoine, P., Dulac, F., and Hatté, C.: Imprint of North-Atlantic abrupt climate changes on western European loess deposits as viewed in a dust emission model, *Quaternary Science Reviews*, 28, 2851–2866, <http://dx.doi.org/10.1016/j.quascirev.2009.07.016>, 2009.

Sima, A., Kageyama, M., Rousseau, D.-D., Ramstein, G., Balkanski, Y., Antoine, P., and Hatté, C.: Modeling dust emission response to North Atlantic millennial-scale climate variations from the perspective of East European MIS 3 loess deposits, *Climate of the Past*, 9, 1385–1402, <https://doi.org/10.5194/cp-9-1385-2013>, <http://dx.doi.org/10.5194/cp-9-1385-2013>, 2013.

Singhvi, A., Bluszcz, A., Bateman, M., and Rao, M.: Luminescence dating of loess–palaeosol sequences and coversands: methodological aspects and palaeoclimatic implications, *Earth-Science Reviews*, 54, 193–211, [http://dx.doi.org/10.1016/S0012-8252\(01\)00048-4](http://dx.doi.org/10.1016/S0012-8252(01)00048-4), 2001.

Stevens, B., Giorgetta, M., Esch, M., Mauritsen, T., Crueger, T., Rast, S., Salzmann, M., Schmidt, H., Bader, J., Block, K., Brokopf, R., Fast, I., Kinne, S., Kornbluh, L., Lohmann, U., Pincus, R., Reichler, T., and Roeckner, E.: Atmospheric component of the MPI-M Earth System Model: ECHAM6, *J. of Advances in Modeling Earth Systems*, 5, 146–172, <https://doi.org/10.1002/jame.20015>, 2013.

Su, L. and Fung, J. C. H.: Sensitivities of WRF-Chem to dust emission schemes and land surface properties in simulating dust cycles during springtime over East Asia, *J. of Geophysical Research: Atmospheres*, 120, 11, <https://doi.org/10.1002/2015JD023446>, 2015.

Sudarchikova, N., Mikolajewicz, U., Timmreck, C., O’Donnell, D., Schurgers, G., Sein, D., and Zhang, K.: Modelling of mineral dust for interglacial and glacial climate conditions with a focus on Antarctica, *Climate of the Past*, 11, 765–779, <http://dx.doi.org/10.5194/cp-11-765-2015>, 2015.

Ugan, A. and Byers, D.: Geographic and temporal trends in proboscidean and human radiocarbon histories during the late Pleistocene, *Quaternary Science Reviews*, 26, 3058–3080, <http://dx.doi.org/10.1016/j.quascirev.2007.06.024>, 2007.

- 548 Újvári, G., Kovács, J., Varga, G., Raucsik, B., and Marković, S. B.: Dust flux estimates for the Last Glacial Period in East Central Europe  
based on terrestrial records of loess deposits: a review, *Quaternary Science Reviews*, 29, 3157–3166, <http://dx.doi.org/10.1016/j.quascirev.2010.07.005>, 2010.
- 550 Újvári, G., Varga, A., Ramos, F. C., Kovács, J., Németh, T., and Stevens, T.: Evaluating the use of clay mineralogy, Sr–Nd isotopes and  
zircon U–Pb ages in tracking dust provenance: An example from loess of the Carpathian Basin, *Chemical Geology*, 304–305, 83–96,  
552 <http://dx.doi.org/10.1016/j.chemgeo.2012.02.007>, 2012.
- Újvári, G., Stevens, T., Molnár, M., Demény, A., Lambert, F., Varga, G., Jull, A. T., Páll-Gergely, B., Buylaert, J.-P., and Kovács, J.: Coupled  
554 European and Greenland last glacial dust activity driven by North Atlantic climate, *Proceedings of the National Academy of Sciences*,  
114, E10632–E10638, <https://doi.org/10.1073/pnas.1712651114>, 2017.
- 556 Varga, G., Kovács, J., and Újvári, G.: Late Pleistocene variations of the background aeolian dust concentration in the Carpathian Basin:  
an estimate using decomposition of grain-size distribution curves of loess deposits, *Netherlands Journal of Geosciences*, 91, 159–171,  
558 <http://dx.doi.org/10.1017/S0016774600001566>, 2012.
- Werner, M.: Seasonal and interannual variability of the mineral dust cycle under present and glacial climate conditions, *J. of Geophysical*  
560 *Research*, 107, <http://dx.doi.org/10.1029/2002JD002365>, 2002.
- Wesely, M.: Parameterization of surface resistances to gaseous dry deposition in regional-scale numerical models, *Atmospheric Environment*  
562 (1967), 23, 1293–1304, [http://dx.doi.org/10.1016/0004-6981\(89\)90153-4](http://dx.doi.org/10.1016/0004-6981(89)90153-4), 1989.
- Willis, K. and van Andel, T.: Trees or no trees? The environments of central and eastern Europe during the Last Glaciation, *Quaternary Sci-*  
564 *ence Reviews*, 23, 2369–2387, <https://doi.org/10.1016/j.quascirev.2004.06.002>, <http://dx.doi.org/10.1016/j.quascirev.2004.06.002>, 2004.
- Yokoyama, Y., Lambeck, K., De Deckker, P., Johnson, P., and Fifield, K.: Timing for the maximum of the Last Glacial constrained by lowest  
566 sea-level observations, *Nature*, 406, 713–716, 2000.
- Zhao, C., Liu, X., Ruby Leung, L., and Hagos, S.: Radiative impact of mineral dust on monsoon precipitation variability over West Africa,  
568 *Atmospheric Chemistry and Physics*, 11, 1879–1893, 2011.
- Zhao, C., Liu, X., and Leung, L.: Impact of the Desert dust on the summer monsoon system over Southwestern North America, *Atmospheric*  
570 *Chemistry and Physics*, 12, 3717–3731, 2012.